

A simple model of reaction induced cracking applied to serpentinization and carbonation of peridotite

John F. Rudge^{a,b,*}, Peter B. Kelemen^b, Marc Spiegelman^b

^a*Institute of Theoretical Geophysics, Bullard Laboratories, University of Cambridge, Madingley Road, Cambridge, CB3 0EZ, UK.*

^b*Lamont-Doherty Earth Observatory, Columbia University, Palisades, New York 10964, USA.*

Abstract

During chemical weathering there is the potential for a positive feedback process to occur: Chemical reactions cause volume changes, increasing stresses and potentially fracturing the rock. In turn, these fractures may enhance transport of chemicals through the rock, accelerating the weathering process. An idealised model of this feedback is presented. Simple scaling laws relate the speed of the weathering front to elastic properties, the rate of transport of reactants, and reaction rates. Five different regimes in the model are identified, although only two of these are appropriate for natural systems, where the reaction rate is a key control on the weathering rate. The model is applied to the carbonation and serpentinization of peridotite, chemical weathering processes which have potential industrial application in the storage of CO₂. If these weathering processes can be accelerated, CO₂ could be stored as carbonates in the peridotite in substantial quantities. This simple model suggests that it may be possible to boost the speed of the weathering front a millionfold by a combination of heating, increased partial pressure of CO₂, forced fluid flow, and hydrofracture.

Key words: Weathering, carbon capture, reaction-diffusion, fracture mechanics

1. Introduction

Chemical weathering is one of the most important processes that shapes the Earth's surface, and yet many aspects of it are still poorly understood. During weathering, a number of distinct physical processes occur, and these processes can interact with one other in interesting ways. Chemical weathering is driven by reactions between the rock and a mobile phase that moves through the rock, such as water, chemicals dissolved in water, or the air. As such the rate of chemical weathering is affected by how well this mobile phase can be transported through the rock, and by how fast it reacts with individual grains within the rock.

The reaction itself can influence the transport of the mobile phase in a variety of ways. One way in which it can do so is by the volume change (expansion or contraction) that can occur as a result of reaction. Volume change can cause increasing stress within the rock, and in turn these stresses can lead to fracturing of the rock, enhancing transport of the mobile

*Corresponding author. Tel: +44 1223 748938. Fax: +44 1223 360779.

Email addresses: rudge@esc.cam.ac.uk (John F. Rudge), peterk@ldeo.columbia.edu (Peter B. Kelemen), mstieg@ldeo.columbia.edu (Marc Spiegelman)

13 phase and thus accelerating weathering (e.g. Fletcher et al., 2006; Malthe-Sørenssen et al.,
14 2006; Rijniers et al., 2005; Flatt et al., 2007; Correns, 1949; Correns and Steinborn, 1939;
15 Scherer, 2004, 1999; Walder and Hallet, 1985; MacDonald and Fyfe, 1985; Jamtveit et al.,
16 2008).

17 The aim of this work is to develop a simple model of the physical processes involved in this
18 particular feedback. To provide a concrete example of chemical weathering, we will discuss the
19 application of the model to hydration and carbonation of peridotite, reactions between surface
20 water and tectonically exposed mantle peridotite to form the hydrous mineral, serpentine, and
21 Mg-Ca-carbonate minerals such as magnesite, dolomite and calcite. Serpentinization is best
22 known as a process of alteration that happens near the seafloor, associated with hydrothermal
23 circulation induced by mid-ocean ridge volcanism, but serpentinization and carbonation also
24 occur via sub-aerial weathering (e.g. Barnes et al., 1967; Barnes and O’Neil, 1969; Bruni et al.,
25 2002; Neal and Stanger, 1985). Weathering of peridotite is of current interest because of its
26 potential for capture and storage of atmospheric CO₂ via mineral carbonation (Kelemen
27 and Matter, 2008; Andreani et al., 2009). Also, serpentinization is an energy source for
28 methanogenic organisms and is thought to be a possible substrate for the origin of life.

29 To make the presentation clearer, the main text describes the model formulation and key
30 results, and detailed derivations are left to the appendices. The approach taken here is based
31 on a simple model for the decomposition of solids developed by Jakobson (1991), which is
32 reviewed in detail in appendix D.1. The problem studied by Jakobson (1991) concerned the
33 decomposition of one solid into another solid plus a mobile gas. The escape of the gas causes a
34 volume decrease in the remaining solid which in turn causes fracturing. The fractures enable
35 the gas to escape more readily and thus the rate of decomposition increases. The model
36 presented here is also closely related to a model for spheroidal weathering (a type of chemical
37 weathering) developed by Fletcher et al. (2006), and a detailed comparison of the two models
38 can be found in appendix D.2. The main difference between the model presented here over
39 that of Fletcher et al. (2006) is that this model is analytically tractable, enabling a better
40 understanding of different behaviours that can occur.

41 Unlike the decomposition problem of Jakobson (1991), which involves volume shrinkage,
42 serpentinization, carbonation, and spheroidal weathering all involve volume expansion. Fluid-
43 rock reactions that increase the solid volume, via reactions with host rock or precipitation
44 of saturated minerals from the fluid, are often self-limiting because they fill porosity, reduce
45 permeability, and create “reaction rims” of solid products that act as diffusive boundary
46 layers between unreacted mineral reactants and fluid (e.g. Aharonov et al. (1998); Milsch
47 et al. (2009); Morrow et al. (2001); Tenthorey et al. (1998)). Decreasing permeability with
48 reaction progress is commonly observed for hydration and carbonation of basalt (Alt and
49 Teagle (1999); Bartetzko (2005); Becker and Davies (2003); Schramm et al. (2005)). On
50 much shorter time and distance scales, experimental dissolution and carbonation of olivine
51 commonly shows a decrease in rate with time due to formation of a “passivating layer” of
52 amorphous SiO₂ on olivine surfaces, after which reaction rate is limited by diffusion through
53 this solid layer (e.g. Chizmeshya et al. (2007)).

54 However, it is also observed that precipitation of super-saturated minerals in pore space
55 can fracture rocks, maintaining permeability and potentially exposing fresh mineral surfaces.
56 For example, salts crystallizing from water in limestone and other building materials can
57 fracture these materials, even while the fluid volume is decreasing (e.g. Scherer (1999, 2004)).
58 Frost heaves and frost cracking are related phenomena (Walder and Hallet, 1985). Similarly,

59 reaction between fluids and minerals that consume fluid components but increase the solid
60 volume, such as hydration of solid lime (CaO) to produce portlandite (Ca(OH)₂), can cause
61 polycrystalline rocks to fracture. Reaction-driven cracking has been observed experimentally
62 in systems undergoing volume expansion, such as in the replacement of leucite by analcime
63 (Jamtveit et al., 2009).

64 Extensive outcrops of serpentinite (completely hydrated peridotite) indicate that serpen-
65 tinization is not always self-limiting. The ubiquitous presence of dense fracture networks in
66 partially serpentinitized peridotite, with fracture spacing ~ 50 microns, much smaller than the
67 original olivine grain size, lends credence to the idea that serpentinitization and cracking are
68 coeval, as do the hierarchical nature of the fracture patterns (Iyer et al., 2008; Jamtveit et al.,
69 2008). Without the presence of serpentine “glue” along these fracture networks, the host
70 would be a powder, rather than a rock.

71 Similarly, the presence of extensive outcrops of listwanite (completely carbonated peri-
72 dotite) in Oman (Nasir et al., 2007; Neal and Stanger, 1985; Stanger, 1985; Wilde et al.,
73 2002) and elsewhere (e.g. Akbulut et al. (2006); Auclair et al. (1993); Hansen et al. (2005);
74 Madu et al. (1990); Naldrett (1966); Robinson et al. (2005); Santti et al. (2006); Schandl
75 and Naldrett (1992); Schandl and Wicks (1993); Ucurum (2000); Ucurum and Larson (1999))
76 demonstrates that olivine carbonation is not always self-limiting, despite increases in the solid
77 volume. Listwanites have brecciated textures in outcrop and dense, hierarchical fracture net-
78 works extending to microscopic scales, filled by syn-kinematic carbonate and quartz veins,
79 probably due to feedback between volume change, stress increase, and fracturing that main-
80 tains permeability and reactive surface area. Outcrop scale and microscopic relationships of
81 carbonate veins in partially carbonated peridotites indicate coeval carbonate crystallization
82 and formation of hierarchical crack networks, and volume expansion of the original host rock
83 to accommodate carbonate precipitation. However, it may be that fracture filling by carbon-
84 ates ultimately did limit reaction progress where we observe partially carbonated rocks. In
85 the model that follows we assume the reaction driven cracking is not self-limiting, although
86 the negative feedbacks which could limit the process should be addressed in future work.

87 2. Model formulation

We consider a simple reaction whereby a mobile phase W (e.g. water or CO₂) reacts with
an immobile solid A (e.g. peridotite) to form an immobile solid product B (e.g. serpentine or
magnesite), $rW + sA \rightarrow B$ where r and s are the stoichiometric coefficients. The two solids
A and B have different densities, and it is this difference in densities that causes stress to
increase in the rock. We model the transport of the mobile phase W by simple diffusion, with
an effective diffusivity D . The solid product B is produced at some rate Q which depends on
the concentrations of the reagents W and A. Let w be the concentration of W (mol m⁻³),
 a be the concentration of A, and b be the concentration of B. We describe the evolution of
these concentrations by the following simple 1D advection-diffusion equations

$$\frac{\partial w}{\partial t} = D \frac{\partial^2 w}{\partial x^2} - rQ, \quad (1)$$

$$\frac{\partial a}{\partial t} = -sQ, \quad (2)$$

$$\frac{\partial b}{\partial t} = Q. \quad (3)$$

88 For simplicity, we assume a first order rate law for Q , namely

$$Q = kwa, \quad (4)$$

89 where k is a rate constant for the reaction ($\text{mol}^{-1} \text{m}^3 \text{s}^{-1}$).

90 We will assume there exists a weathering front that propagates at some velocity v as a
 91 result of the reaction induced cracking (Figure 1). Behind the front it is assumed that the rock
 92 has been cracked, that the stress has been relaxed, and that the mobile phase concentration is
 93 maintained at some fixed level w_0 (e.g. because it is in contact with a reservoir of the mobile
 94 phase and there is rapid flow through the cracked rock). Far ahead of the front it is assumed
 95 that there is no mobile phase, the rock is uncracked, and that there is only the reactant solid
 96 A at some concentration a_0 . The mobile phase diffuses into the uncracked rock, reacting as
 97 it goes.

In a frame moving with the front, the reaction-diffusion equations (1-3) become

$$-v \frac{dw}{dx} = D \frac{d^2w}{dx^2} - rQ, \quad (5)$$

$$-v \frac{da}{dx} = -sQ, \quad (6)$$

$$-v \frac{db}{dx} = Q, \quad (7)$$

with boundary conditions

$$w(0) = w_0, \quad w(\infty) = 0, \quad (8)$$

$$a(\infty) = a_0, \quad (9)$$

$$b(\infty) = 0, \quad (10)$$

98 where $x = 0$ is the position of the front in the moving frame and $x = \infty$ is a position far
 99 ahead of the weathering front. We will define $b_0 = a_0/s$, i.e. the concentration of solid B that
 100 would be produced if all of solid A were reacted. It is helpful also to define $\kappa = skw_0$, a rate
 101 constant (s^{-1}) for the production of solid B in the presence of a concentration w_0 of water.
 102 Note that (6), (7), (9), and (10) imply that $a = s(b_0 - b)$, and thus we only need solve for w
 103 and b . The reaction rate Q is then given by (4) as

$$Q = \kappa \frac{w}{w_0} (b_0 - b), \quad (11)$$

104 where $\kappa = skw_0$.

105 As the reaction proceeds, stress builds up in the rock due to the volume change. We will
 106 assume production of B ahead of the front produces stresses σ in a simple linear fashion as

$$\sigma = \beta Eb/b_0, \quad (12)$$

107 where E is the Young's modulus of the uncracked rock, and β is a non-dimensional prefactor
 108 that relates to the amount of volume change as

$$\beta = \frac{1}{3(1-\nu)} \frac{\Delta V}{V}. \quad (13)$$

109 Here ν is Poisson's ratio, and $\Delta V/V$ is the relative volume change that occurs when all of
110 solid A reacts to produce solid B.

111 Finally, we must relate the build up of stress to the fracturing that drives the weathering
112 front forward. We do this using a highly simplified fracture criterion, motivated by the linear
113 fracture mechanics of a single crack. Suppose we have a crack of length L and apply a
114 uniform stress σ over the crack faces. Then the crack will grow when the stress intensity
115 factor K exceeds some critical value, known as the fracture toughness K_c ($\text{Pa m}^{1/2}$). To a
116 first approximation, the stress intensity factor K is related to the applied stress and crack
117 length through $K = \sigma L^{1/2}$. In detail there is a numerical prefactor that depends on the
118 particular geometry and type of loading, but we shall not concern ourselves with this as our
119 main interest is in overall scalings.

120 The rate of advance of the weathering front by fracturing should be determined by the
121 stress field ahead of the front, $\sigma(x)$. To generate an appropriate fracture criterion we make
122 three assumptions: Firstly, we assume a steadily propagating front, so that the cracks near
123 the front are in a state of quasi-equilibrium and the stress intensity factor takes the critical
124 value, $K = K_c$. Second, we hypothesise that the typical crack length L is determined by a
125 typical length scale over which the stress field $\sigma(x)$ decays: formally, we let L be the length
126 over which σ reaches 37% ($1/e$) of its value at the front. Finally, we assume that the value
127 of σ at the front provides a good estimate for the loading on the cracks. Thus the fracture
128 criterion we assume is

$$K_c = \sigma(0) L^{1/2}. \quad (14)$$

129 By combining (12) and (14), the fracture criterion can be written as

$$K_c = \beta E L^{1/2} b(0)/b_0, \quad (15)$$

130 where the crack length L is chosen to be the length scale over which $b(x)$ decays (the value
131 of x for which it reaches $1/e$ of its value at the front, [Figure 1b](#)).

132 A fracture criterion, like that of (15), is necessary to close the equations and relate the
133 reaction-diffusion problem to the fracturing. Similar criterion have been used in the models
134 of [Yakobson \(1991\)](#) and [Fletcher et al. \(2006\)](#) ([Appendix D](#)). In the case of [Yakobson \(1991\)](#)'s
135 model, the stress intensity factor K is calculated for a single crack of length L subject to a
136 loading $\sigma(x)$ on the crack faces, with K again assumed equal to the fracture toughness $K = K_c$.
137 A dynamical hypothesis is made that the front propagates at its maximum possible velocity,
138 and in order to do this it is found that the crack length scale L must be the length scale over
139 which $\sigma(x)$ decays (up to some order 1 constants). In the model of [Fletcher et al. \(2006\)](#), the
140 reaction ceases once the mobile phase concentration drops below a certain threshold, and the
141 distance to this threshold determines the typical crack spacing. Thus the crack spacing in the
142 model of [Fletcher et al. \(2006\)](#) is also set by a length scale in the reaction-diffusion problem,
143 although this length scale is that of the mobile phase concentration profile rather than the
144 product concentration profile. However, in many situations these length scales are the same
145 (see [Appendix D](#) for further discussion). The fracture criterion of [Fletcher et al. \(2006\)](#) is
146 written in terms of surface energy of fracture, and this can be directly related to the fracture
147 toughness.

148 The above equations (5-15) describe a simple model of a steadily propagating weathering
149 front caused by volume changes due to reaction. The main aim of the analysis is to determine
150 the front velocity v and the typical crack length L as a function of the given parameters.

151 **3. Results**

152 A detailed analysis of the equations above are presented in appendices A to C, and we
 153 summarise the main results of the analysis in this section. The behaviour of the model is
 154 determined by just two non-dimensional parameters, Λ and Θ , defined by

$$\Lambda = \frac{\kappa}{D} \left(\frac{K_c}{\beta E} \right)^4, \quad \Theta = \frac{w_0}{rb_0}. \quad (16)$$

155 Λ relates the rate of reaction (κ), rate of transport (D), elastic properties (K_c and E), and
 156 volume change factor (β). Λ large means either rapid reaction, slow transport of mobile phase,
 157 tougher to fracture, or small volume changes. Θ is simply a concentration ratio, adjusted for
 158 stoichiometry. Large Θ simply means large amounts of mobile phase relative to solid.

The aim of the analysis is to find relationships for the weathering front velocity v and the characteristic crack length L . These can be expressed in terms of non-dimensional functions $\zeta(\Lambda, \Theta)$ and $\eta(\Lambda, \Theta)$ as

$$L = \left(\frac{K_c}{\beta E} \right)^2 \zeta(\Lambda, \Theta), \quad (17)$$

$$v = D \left(\frac{\beta E}{K_c} \right)^2 \eta(\Lambda, \Theta). \quad (18)$$

159 The length scale $(K_c/\beta E)^2$ is a natural length scale associated with fracture caused by volume
 160 change. In fact, this length scale provides a lower bound for L . $D(\beta E/K_c)^2$ provides a natural
 161 velocity scale.

162 The two non-dimensional functions $\eta(\Lambda, \Theta)$ and $\zeta(\Lambda, \Theta)$ have been calculated numerically
 163 for a range of Λ and Θ , and contour plots of the functions are shown in Figures 2 and 3. The
 164 main features of these plots are straightforward to understand when we interpret Λ as a non-
 165 dimensional reaction rate and Θ as a non-dimensional water concentration. Non-dimensional
 166 front velocity $\eta(\Lambda, \Theta)$ increases with increasing Λ and increasing Θ , which reflects the fact
 167 that the weathering front moves faster if the reaction happens faster or if there is more water
 168 present. Non-dimensional crack length $\zeta(\Lambda, \Theta)$ increases with decreasing Λ , which reflects the
 169 fact that we get longer cracks with slower reactions (since slower reactions allow more time
 170 for the water to diffuse further past the front). $\zeta(\Lambda, \Theta)$ also increases with increasing Θ , as
 171 more water present also allows transport further past the front.

172 While the functions $\eta(\Lambda, \Theta)$ and $\zeta(\Lambda, \Theta)$ can be calculated numerically, it will often be
 173 the case that the non-dimensional parameters Λ and Θ are large or small. In such cases,
 174 there are some simple analytical expressions for the forms of $\eta(\Lambda, \Theta)$ and $\zeta(\Lambda, \Theta)$, and the
 175 corresponding dimensional expressions for v and L are shown in Table 1. Based on the relative
 176 magnitudes of Λ and Θ , the parameter space divides into five asymptotic regimes as shown
 177 in Figure 4.

178 Some aspects of the asymptotic regimes have clear physical interpretations. For example,
 179 regimes 4 and 5 represent very rapid reaction, and the corresponding results are independent
 180 of the rate constant κ . In these regimes all the solid reactant is used up, and the fracture scale
 181 reaches its lower limit (known as “brittle fracturing”). In regime 3 there is weak (logarithmic)
 182 dependence on the reaction rate κ , but the fracture scale is still that of brittle fracturing and all
 183 the solid reactant is still used up. In regimes 1 and 2 the reaction is slow and limits the speed at

184 which the front can propagate (“reaction controlled”). The front velocity still depends on the
 185 elastic properties and the diffusivity of the mobile phase, but more weakly. The corresponding
 186 fracture scales are larger, and in regime 1, the crack length L is completely independent of
 187 the elastic properties. The difference between regimes 1 and 2 is best understood in terms of
 188 the dependence on Θ : In regime 1, Θ is small and propagation of the front is limited by the
 189 availability of water. Regime 2 has larger Θ and front propagation is no longer controlled by
 190 the availability of water as it is plentiful, and this is reflected in the expressions for v and L
 191 which are independent of Θ . Similarly, the expressions in regime 3 are independent of Θ , and
 192 the transition from regime 3 to regime 4 reflects the point at which the availability of water
 193 again becomes a controlling factor.

194 4. Serpentinization and carbonation of peridotite

195 The model may be useful in understanding some of the controls on the rate of serpentiniza-
 196 tion and carbonation of peridotite during weathering. In turn, this understanding could be
 197 valuable in designing systems for enhanced, in situ carbonation of peridotite for CO_2 capture
 198 and storage. Unfortunately, a number of the model parameters are not well known, notably
 199 the rate of transport of water (D), and this makes applying the model to real situations
 200 difficult. However, some useful order of magnitude estimates can be made.

201 The elastic properties of peridotite are fairly well known, with a Young’s modulus $E \sim 10^{11}$
 202 Pa and fracture toughness $K_c \sim 10^6$ Pa m^{1/2}. A typical volume expansion is around 20%,
 203 leading to $\beta \sim 0.13$ for a Poisson’s ratio $\nu \sim 0.25$. The reaction rate κ can be estimated
 204 from experimental data. Though experiments are done on powder, inferences can be made
 205 on the reactive surface area in powder versus the grain size in a rock that allows scaling
 206 of the experimental data to a natural situation. The parameterisations of carbonation and
 207 serpentinization rate used are those of [Kelemen and Matter \(2008\)](#).

208 For serpentinization, the experimental data of [Martin and Fyfe \(1970\)](#) was parameterised
 209 as

$$\kappa_{\text{serp.}} = \kappa_0 \left(\frac{a_0}{a}\right)^2 e^{-\alpha(T-T_0)^2}, \quad (19)$$

210 where $\kappa_0 = 10^{-6}$ s⁻¹, $a_0 = 70$ μm , $\alpha = 2.09 \times 10^{-4}$ °C⁻², $T_0 = 260$ °C. The experiments were
 211 performed with 70 μm grains, and the factor $(a_0/a)^2$ reflects the scaling due to surface area
 212 effects, where a is the typical grain size controlling the reaction. T_0 is the temperature at
 213 which the serpentinization rate reaches its peak, and κ_0 is the corresponding peak rate for 70
 214 μm grains.

215 For carbonation, the experimental data of [O’Connor et al. \(2005\)](#) was parameterised as

$$\kappa_{\text{carb.}} = \kappa_0 \left(\frac{a_0}{a}\right)^2 \left(\frac{P_{\text{CO}_2}}{P_0}\right)^{1/2} e^{-\alpha(T-T_0)^2}, \quad (20)$$

216 where $\kappa_0 = 1.15 \times 10^{-5}$ s⁻¹, $a_0 = 70$ μm , $P_0 = 1$ bar, $\alpha = 3.34 \times 10^{-4}$ °C⁻², $T_0 = 185$ °C.
 217 There is an additional influence on the carbonation rate due to the partial pressure P_{CO_2} of
 218 carbon dioxide. Here, κ_0 is the peak reaction rate at a reference partial pressure P_0 of 1 bar,
 219 again with 70 μm grains.

220 Typical summer temperatures in Oman are around $T \sim 50$ °C. Typical grain sizes of
 221 peridotite are around $a \sim 0.1$ mm, and a similar value is obtained for estimates of crack

222 spacing in crystalline rocks that are roughly similar to peridotite (Sprunt and Brace, 1974;
 223 Brace, 1977; Wong et al., 1989). Typical partial pressures are around $P_{\text{CO}_2} \sim 4 \times 10^{-4}$ bars.
 224 Thus estimated natural reaction rates are $\kappa_{\text{serp.}} \sim 5 \times 10^{-11} \text{ s}^{-1}$ for serpentinization, and
 225 $\kappa_{\text{carb.}} \sim 2.5 \times 10^{-10} \text{ s}^{-1}$ for carbonation.

226 The speed of the weathering front in the Oman ophiolite has been estimated at $v \sim 0.3$
 227 mm yr^{-1} (Poupeau et al., 1998), which is in keeping with the observation that the average ^{14}C
 228 age of carbonate veins in peridotite exposed to weathering in Oman, in a weathering horizon
 229 $\sim 10 \text{ m}$ thick, is about 26,000 years (Kelemen and Matter, 2008).

230 Assuming asymptotic regime 1, the expressions for v and L are (Table 1)

$$v = \frac{\beta E}{K_c} \kappa^{1/4} (D\Theta)^{3/4}, \quad L = \left(\frac{D\Theta}{\kappa} \right)^{1/2}, \quad (21)$$

231 which are valid provided

$$\Theta^4 \ll \frac{\Lambda}{\Theta} \ll 1, \quad (22)$$

232 which has to be checked. Since we have a reasonable estimate for v , the above equations
 233 can be rearranged to provide expressions for the effective diffusivity D required to match the
 234 observed weathering rate,

$$D\Theta = \left(\frac{K_c v}{\beta E} \right)^{4/3} \kappa^{-1/3}, \quad (23)$$

235 and corresponding expressions for L and Λ/Θ are

$$L = \left(\frac{K_c v}{\beta E \kappa} \right)^{2/3}, \quad \frac{\Lambda}{\Theta} = \frac{\kappa}{D\Theta} \left(\frac{K_c}{\beta E} \right)^4. \quad (24)$$

236 Using the carbonation rate $\kappa_{\text{carb.}}$, the estimates above imply $D\Theta \sim 10^{-17} \text{ m}^2 \text{ s}^{-1}$ and a
 237 typical crack length scale $L \sim 0.2 \text{ mm}$ (very similar to the proposed grain size $a \sim 0.1 \text{ mm}$).
 238 $\Lambda/\Theta = 8 \times 10^{-10}$ which is certainly much less than 1 (as required by (22)), and will be
 239 greater than Θ^4 , provided $\Theta < 0.005$. Since the estimates above are only weakly dependent
 240 on κ (dependences of $\kappa^{-1/3}$ and $\kappa^{-2/3}$), using the serpentinization rate $\kappa_{\text{serp.}}$ instead (with its
 241 factor of 5 slower rate), produces fairly similar estimates.

242 Θ represents a ratio of mobile phase concentration to solid reactant concentration, which
 243 can be estimated based on the amount of water that can be stored on grain boundaries or
 244 microcracks in the rock. Laboratory-based estimates of grain boundary width in crystalline
 245 rocks are around $w \sim 0.01 \mu\text{m}$ (Farver and Yund, 1992; Yund, 1997; Farver and Yund, 1991),
 246 which provide estimates of porosity $\phi \sim 3w/a = 3 \times 10^{-4}$. Taking this porosity ϕ as an
 247 estimate for Θ yields an effective diffusivity $D \sim 3 \times 10^{-14} \text{ m}^2 \text{ s}^{-1}$ using (23). The effective
 248 diffusivity D encompasses a number of different processes that cause the mobile phase to
 249 be transported through the rock, including advection, diffusion, and dispersion, and is a
 250 difficult quantity to estimate directly. However, the required value of D is fairly similar to
 251 that expected from experimental measurements of diffusion of water-in-water $D_{\text{water-in-water}} \sim$
 252 $6 \times 10^{-11} \text{ m}^2 \text{ s}^{-1}$ (Farver and Yund (1992), extrapolated to 50°C), which when multiplied by
 253 ϕ gives an effective diffusivity $D \sim 2 \times 10^{-14} \text{ m}^2 \text{ s}^{-1}$, very close to the required value.

254 For practical industrial storage of CO_2 we would like to increase the front velocity v ,

$$v = \frac{\beta E}{K_c} \kappa^{1/4} (D\Theta)^{3/4}, \quad (25)$$

255 by many orders of magnitude. To do this we can either increase the reaction rate (κ), in-
 256 crease the transport of mobile phase (D), or increase the availability of mobile phase (Θ).
 257 It is possible to estimate the order of magnitude increases in front velocity one can expect
 258 under different engineered conditions. One of the simplest ways of accelerating the weather-
 259 ing process is by heating: at the optimal temperature for carbonation (185°C), the rate of
 260 carbonation is 450 times greater than it is at 50°C. However, since the front velocity depends
 261 only weakly on κ , this leads to only a 5 fold increase in front velocity. Temperature will also
 262 influence the effective diffusivity of the mobile phase. Based on the temperature dependence
 263 of water-in-water diffusion of [Farver and Yund \(1992\)](#), this could be expected to increase D
 264 by around a factor of 5, which leads to another 3 fold increase in v . Hence heating overall
 265 could potentially lead to a 15 times greater front velocity. Such heating may be self sustaining
 266 due to the exothermic nature of the serpentinization and carbonation reactions ([Kelemen and](#)
 267 [Matter, 2008](#)).

268 The kinetics of carbonation are very dependent on the partial pressure of CO₂, and in-
 269 creasing this is another way to speed the front. An increase in P_{CO_2} to 300 bars would lead
 270 to a 900 fold increase in the carbonation rate, and a corresponding 5 fold increase in front
 271 velocity. Thus heating and elevated partial pressure combined could lead to a 75 times faster
 272 front velocity, which is still somewhat short of what one would like for industrial applications.

273 According to (25), the effective diffusivity D (which describes the transport of the mobile
 274 phase through the rock), and Θ (which describes the availability of water) have a much greater
 275 influence on the front velocity than κ (the reaction rate). $D\Theta$ will need to be increased
 276 by orders of magnitude to produce industrially viable solutions. One way of doing this is
 277 by increasing the porosity, which could be done by hydrofracturing the rock at depth. An
 278 increase in porosity to 1% (typical for cracked rock, e.g. [Wu et al. \(2006\)](#)) could be expected
 279 to produce a 200 fold increase in front velocity.

280 However, even larger effective diffusivities may be possible if the flow is forced by applying
 281 a pressure gradient. Rapid fluid flow within the fractures will cause enhanced concentration
 282 gradients and thus increase the effective diffusivity. A rough estimate of the effective diffusivity
 283 for forced flow in cracked rock is $D \approx \phi v_{\text{crack}} \alpha$ where ϕ is the porosity, v_{crack} is the fluid velocity
 284 in the crack, and α is a dispersivity parameter ([Wu et al., 2009](#)). Darcy velocities $\phi v_{\text{crack}} \sim$
 285 10^{-4} m s^{-1} can be generated with moderate pressure gradients (a typical permeability of
 286 cracked rock is $k \sim 10^{-12} \text{ m}^2$, [Wu et al. \(2006\)](#)), and a crude estimate of the dispersivity
 287 parameter can be obtained from a typical crack width, $\alpha \sim 2 \times 10^{-5} \text{ m}$. These estimates lead
 288 to effective diffusivities $D \sim 2 \times 10^{-9} \text{ m}^2 \text{ s}^{-1}$, 70'000 larger than the inferred natural effective
 289 diffusivity, and producing a 4'000 fold increase in front velocity. With a combination of all
 290 the above suggestions, it may be possible to go from the natural weathering rate of tenths of
 291 millimetres a year to an industrial rate of hundreds of metres a year.

292 In estimating the front velocities under engineered circumstances, it was assumed that
 293 regime 1 held throughout (equation (25) was used), and this assumption should be checked.
 294 The natural estimates have $\Lambda \sim 2 \times 10^{-13}$. The largest Λ in the engineered circumstances is
 295 when the reaction rate κ alone is increased (see (16)). An increase in κ by a factor of 4×10^5
 296 (i.e. heating and increased partial pressure) gives $\Lambda \sim 8 \times 10^{-8}$. This value of Λ certainly
 297 satisfies $\Lambda \ll 1$ and $\Lambda \ll \Theta$ for any reasonable value of Θ , and hence only regimes 1 or 2 are
 298 ever appropriate ([Table 1](#)). If $\Theta^5 \ll \Lambda$ we are in regime 1; if $\Theta^5 \gg \Lambda$ we are in regime 2. In the
 299 natural situation, it was estimated that $\Theta \sim 3 \times 10^{-4}$ and thus $\Theta^5 \sim 2 \times 10^{-18}$, and regime 1 is
 300 appropriate. However, in the engineered situations where porosity is increased $\Theta \sim 0.01$ and

301 thus $\Theta^5 \sim 10^{-10}$, which is greater than Λ in some scenarios. Hence regime 2 is a possibility
302 in some engineered conditions, where water is plentiful and the front velocity v becomes
303 independent of Θ . However, the velocities estimated by the regime 1 and 2 equations differ by
304 only $(\Lambda/\Theta^5)^{3/20}$, which at most a factor of 2 for the scenarios in which regime 2 expressions
305 are appropriate, so this does not change the results greatly.

306 In oceanic settings, rates of serpentinization are very poorly known. One pertinent obser-
307 vation is that peridotites exposed on the seafloor at and near mid-ocean ridges are invariably,
308 partially to completely serpentinized. No significant gradient in the degree of serpentinization
309 is observed as a function of depth in drill holes extending for 100 to 200 meters (Bach et al.,
310 2004; Kelemen et al., 2004, 2007; Paulick et al., 2006). Tectonically induced faults and shear
311 zones are common in this environment. Once formed, these features could enhance the rate
312 of serpentinization in peridotites near the seafloor, yet they have nothing to do with reaction-
313 induced cracking. However, seismic data suggest a gradient of decreasing serpentinization
314 that extends downward from the seafloor over ~ 5 km in some places (Figure F5, Chapter 1,
315 Kelemen et al. (2004)). The presence of such a gradient suggests generally continuous, down-
316 ward transport of water through a fracture network, rather than localized transport along a
317 few large faults. Though these and other, similar observations were made at slow-spreading
318 ridges, where rates of uplift and tectonic denudation are slow, at least some of the peridotites
319 exposed on the seafloor must have approached the seafloor within the past 10^6 years, if not
320 less. Thus a minimum rate for propagation of a serpentinization front in oceanic crust might
321 be $v \sim 5$ mm yr $^{-1}$ (around a factor of 10 faster than the Oman weathering rate), and the
322 actual rates could be orders of magnitude faster. Applying the model in this setting, with
323 a kinetic rate $\kappa_{\text{serp.}} \sim 5 \times 10^{-11}$ s $^{-1}$, implies lower bounds of $D\Theta \sim 8 \times 10^{-16}$ m 2 s $^{-1}$ and
324 $L \sim 0.4$ mm, very similar to the values calculated for Oman peridotite weathering, although
325 these values could be much larger if the front velocities are orders of magnitude faster.

326 5. Conclusion

327 The main results of this work are presented in Table 1, which show how the speed and mor-
328 phology of a chemical weathering front depends on the rate of reaction, rate of fluid transport,
329 elastic properties, and amount of volume change, within the framework of a highly idealised
330 model. For realistic parameter values, only regimes 1 and 2 will be observed (“reaction con-
331 trolled regimes”). The model predicts the velocity of a reaction-driven cracking front in rocks
332 undergoing volume change due to fluid-rock interaction, and the simple scalings that result
333 are the first step towards understanding the behaviour of more sophisticated models. There
334 are many avenues for future work on this problem. It would be very useful to look further
335 at 2D problems (e.g. Malthe-Sørenssen et al. (2006); Røyne et al. (2008)), where the elastic
336 stress field and its boundary conditions can be modelled more carefully, and a better treat-
337 ment of the fracture criterion could then be attempted. As mentioned in the introduction,
338 there are potential negative feedbacks that may limit the reaction driven cracking which are
339 not included in this model, and should be explored in future. Notably, the volume expanding
340 reaction may clog the pore space and hinder transport of the mobile phase rather than aiding
341 transport by fracturing (e.g. Andreani et al. (2009)). This feedback may be possible to study
342 in a 1D model using an evolution equation for permeability: work on this is ongoing.

343 **Acknowledgements**

344 We thank the editor Yanick Ricard and three anonymous reviewers for their valuable
345 comments. We also thank David Bercovici for many useful discussions. This work was
346 supported by NSF grants OCE-0452457 and EAR-0610138.

347 **References**

- 348 Aharonov, E., Tenthorey, E., Scholz, C. H., 1998. Precipitation sealing and diagenesis 2. The-
349 oretical analysis. *J. Geophys. Res.* 103, 23969–23981. doi:10.1029/98JB02230.
- 350 Akbulut, M., Piskin, O., Karayigit, A. I., 2006. The genesis of the carbonatized and silicified
351 ultramafics known as listvenites: A case study from the Mihaliccik region (Eskisehir), NW
352 Turkey. *Geol. J.* 41, 557–580. doi:10.1002/gj.1058.
- 353 Alt, J. C., Teagle, D. A. H., 1999. The uptake of carbon during alteration of oceanic crust.
354 *Geochim. Cosmochim. Acta* 63, 1527–1535. doi:10.1016/S0016-7037(99)00123-4.
- 355 Andreani, M., Luquot, L., Gouze, P., Godard, M., Hois, E., Gibert, B., 2009. Experimental
356 study of carbon sequestration reactions controlled by the percolation of CO₂-rich brine
357 through peridotites. *Environ. Sci. Technol.* 43, 1226–1231. doi:10.1021/es8018429.
- 358 Auclair, M., Gauthier, M., Trottier, J., Jébrak, M., Chartrand, F., 1993. Mineralogy, geo-
359 chemistry, and paragenesis of the Eastern Metals serpentinite-associated Ni-Cu-Zn deposit,
360 Quebec Appalachians. *Econ. Geol.* 88, 123–138. doi:10.2113/gsecongeo.88.1.123.
- 361 Bach, W., Garrido, C.-J., Paulick, H., Harvey, J., Rosner, M., Party, S. S., 2004. Seawater-
362 peridotite interactions: First insights from ODP Leg 209, MAR 15°N. *Geochem. Geophys.*
363 *Geosyst.* 5, Q09F26. doi:10.1029/2004GC000744.
- 364 Barnes, I., LaMarche, V. C., Himmelberg, G., 1967. Geochemical evidence of present-day
365 serpentinization. *Science* 156, 830–832. doi:10.1126/science.156.3776.830.
- 366 Barnes, I., O’Neil, J. R., 1969. Relationship between fluids in some fresh alpine-type ultra-
367 mafics and possible modern serpentinization, western United States. *GSA Bull.* 80, 1947–
368 1960. doi:10.1130/0016-7606(1969)80[1947:TRBFIS]2.0.CO;2.
- 369 Bartetzko, A., 2005. Effect of hydrothermal ridge flank alteration on the in situ physical
370 properties of oceanic crust. *J. Geophys. Res.* 110, B06203. doi:10.1029/2004JB003228.
- 371 Becker, K., Davies, E., 2003. New evidence for age variation and scale effects of permeabilities
372 of young oceanic crust from borehole thermal and pressure measurements. *Earth Planet.*
373 *Sci. Lett.* 210, 499–508. doi:10.1016/S0012-821X(03)00160-2.
- 374 Boeck, T., Bahr, H. A., Lampenscherf, S., Bahr, U., 1999. Self-driven propagation of crack
375 arrays: A stationary two-dimensional model. *Phys. Rev. E* 59, 1408–1416. doi:10.1103/
376 *PhysRevE*.59.1408.
- 377 Brace, W. F., 1977. Permeability from resistivity and pore shape. *Geophys. Res. Lett.* 82,
378 3343–3349.

- 379 Bruni, J., Canepa, M., Chiodini, G., Cioni, R., Cipolli, F., Longinelli, A., Marini, L., Ot-
380 tonello, G., Zuccolini, M. V., 2002. Irreversible water-rock mass transfer accompanying
381 the generation of the neutral, MgHCO_3 and high-pH, CaOH spring waters of the Genova
382 province, Italy. *Applied Geochem.* 17, 455–474. doi:10.1016/S0883-2927(01)00113-5.
- 383 Chizmeshya, A. V. G., McKelvy, M. J., Squires, K., Carpenter, R. W., Béarat, H., 2007. DOE
384 Final Report 924162. A novel approach to mineral carbonation: Enhancing carbonation
385 while avoiding mineral pretreatment process cost. Tech. rep., Tempe, AZ, Arizona State
386 University.
- 387 Correns, C. W., 1949. Growth and dissolution of crystals under linear pressure. *Discuss.*
388 *Faraday Soc.* 5, 267–271.
- 389 Correns, C. W., Steinborn, W., 1939. Experimente zur messung and erklärung der sogenannten
390 kristallisationskraft. *Zeit. Krist.* 101, 117–133.
- 391 Farver, J. R., Yund, R. A., 1991. Measurement of oxygen grain boundary diffusion in natural,
392 fine-grained, quartz aggregates. *Geochim. Cosmochim. Acta* 55, 1597–1607. doi:10.1016/
393 0016-7037(91)90131-N.
- 394 Farver, J. R., Yund, R. A., 1992. Oxygen diffusion in a fine-grained quartz aggregate with
395 wetted and non-wetted microstructures. *J. Geophys. Res.* 97, 14017–14029. doi:10.1029/
396 92JB01206.
- 397 Flatt, R. J., Steiger, M., Scherer, G. W., 2007. A commented translation of the paper by
398 C. W. Correns and W. Steinborn on crystallization pressure. *Environ. Geol.* 52, 187–203.
399 doi:10.1007/s00254-006-0509-5.
- 400 Fletcher, R., Buss, H., Brantley, S., 2006. A spheroidal weathering model coupling porewater
401 chemistry to soil thicknesses during steady-state denudation. *Earth Planet. Sci. Lett.* 244,
402 444–457. doi:10.1016/j.epsl.2006.01.055.
- 403 Hansen, L. D., Dipple, G. M., Gordon, T. M., Kellet, D. A., 2005. Carbonated serpentinite
404 (listwanite) at Atlin, British Columbia: A geological analogue to carbon dioxide sequestra-
405 tion. *Can. Mineral.* 43, 225–239. doi:10.2113/gscanmin.43.1.225.
- 406 Iyer, K., Jamtveit, B., Mathiesen, J., Malthe-Sørenssen, A., Feder, J., 2008. Reaction-assisted
407 hierarchical fracturing during serpentinization. *Earth Planet. Sci. Lett.* 267, 503–516. doi:
408 10.1016/j.epsl.2007.11.060.
- 409 Jamtveit, B., Malthe-Sørenssen, A., Kostenko, O., 2008. Reaction enhanced permeability
410 during retrogressive metamorphism. *Earth Planet. Sci. Lett.* 267, 620–627. doi:10.1016/
411 j.epsl.2007.12.016.
- 412 Jamtveit, B., Putnis, C. V., Malthe-Sørenssen, A., 2009. Reaction induced fracturing
413 during replacement processes. *Contrib. Mineral. Petrol.* 157, 127–133. doi:10.1007/
414 s00410-008-0324-y.
- 415 Kelemen, P. B., Kikawa, E., Miller, D. J., 2004. Proc. ODP, Init. Repts. 209. Tech. rep.,
416 College Station, TX, Ocean Drilling Program. doi:10.2973/odp.proc.ir.209.101.2004.

- 417 Kelemen, P. B., Kikawa, E., Miller, D. J., Party, S. S., 2007. Processes in a 20-km-thick
418 conductive boundary layer beneath the Mid-Atlantic Ridge, 14°-16°N. In: Proc. ODP, Sci.
419 Results, 209. College Station, TX, Ocean Drilling Program, pp. 1–33. [doi:10.2973/odp.
420 proc.sr.209.001.2007](https://doi.org/10.2973/odp.proc.sr.209.001.2007).
- 421 Kelemen, P. B., Matter, J. M., 2008. In situ carbonation of peridotite for CO₂ storage. Proc.
422 Nat. Acad. Sci. USA 105, 17295–17300. [doi:10.1073/pnas.0805794105](https://doi.org/10.1073/pnas.0805794105).
- 423 MacDonald, A. H., Fyfe, W. S., 1985. Rate of serpentinization in sea-floor environments.
424 Tectonophysics. 116, 123–135. [doi:10.1016/0040-1951\(85\)90225-2](https://doi.org/10.1016/0040-1951(85)90225-2).
- 425 Madu, B. E., Nesbitt, B. E., Muehlenbachs, K., 1990. A mesothermal gold-stibnite-quartz
426 vein occurrence in the Canadian Cordillera. Econ. Geol. 85, 1260–1268. [doi:10.2113/
427 gsecongeo.85.6.1260](https://doi.org/10.2113/gsecongeo.85.6.1260).
- 428 Malthe-Sørenssen, A., Jamtveit, B., Meakin, P., 2006. Fracture patterns generated by dif-
429 fusion controlled volume changing reactions. Phys. Rev. Lett. 96, 245501. [doi:10.1103/
430 PhysRevLett.96.245501](https://doi.org/10.1103/PhysRevLett.96.245501).
- 431 Martin, B., Fyfe, W. S., 1970. Some experimental and theoretical observations on the kinetics
432 of hydration reactions with particular reference to serpentinization. Chem. Geol. 6, 185–202.
433 [doi:10.1016/0009-2541\(70\)90018-5](https://doi.org/10.1016/0009-2541(70)90018-5).
- 434 Milsch, H., Seibt, A., Spangenberg, E., 2009. Long-term petrophysical investigations on
435 geothermal reservoir rocks at simulated in situ conditions. Transp. Porous Med. 77, 59–
436 78. [doi:10.1007/s11242-008-9261-5](https://doi.org/10.1007/s11242-008-9261-5).
- 437 Morrow, C., Moore, D., Lockner, D., 2001. Permeability reduction in granite under hydrother-
438 mal conditions. J. Geophys. Res. 106, 30551–30560. [doi:10.1029/2000JB000010](https://doi.org/10.1029/2000JB000010).
- 439 Naldrett, A. J., 1966. Talc-carbonate alteration of some serpentinized ultramafic rocks south
440 of Timmins, Ontario. J. Petrol. 7, 489–499.
- 441 Nasir, S., Al Sayigh, A. R., Al Harthy, A., Al-Khirbash, S., Al-Jaaidi, O., Musllam, A.,
442 Al-Mishwat, A., Al-Bu'saidi, S., 2007. Mineralogical and geochemical characterization of
443 listwaenite from the Semail ophiolite, Oman. Chemie Der Erde - Geochem. 67, 213–228.
444 [doi:10.1016/j.chemer.2005.01.003](https://doi.org/10.1016/j.chemer.2005.01.003).
- 445 Neal, C., Stanger, G., 1985. Past and present serpentinization of ultramafic rocks: An example
446 from the Semail ophiolite nappe of northern Oman. In: The Chemistry of Weathering. D.
447 Reidel Publishing Company, Holland, pp. 249–275.
- 448 O'Connor, W., Dahlin, D., Rush, G., Gerdemann, S., Penner, L., Nilsen, D., 2005. Final
449 report: Aqueous mineral carbonation. Mineral availability, pretreatment, reaction para-
450 metrics, and process studies, Report DOE/ARC-TR-04-002. Tech. rep., Office of Process
451 Development, Albany Research Center, Office of Fossil Energy, US DOE, Albany, OR.
- 452 Paulick, H., Bach, W., Godard, M., Hoog, J. C. M. D., Suhr, G., Harvey, J., 2006. Geo-
453 chemistry of abyssal peridotites (Mid-Atlantic Ridge, 15°20'N, ODP Leg 209): Implica-
454 tions for fluid/rock interaction in slow spreading environments. Chem. Geol. 234, 179–210.
455 [doi:10.1016/j.chemgeo.2006.04.011](https://doi.org/10.1016/j.chemgeo.2006.04.011).

- 456 Poupeau, G., Saddiqi, O., Michard, A., Goffé, B., Oberhänsli, R., 1998. Late thermal evolution
457 of the Oman Mountains subophiolitic windows: Apatite fission-track thermochronology.
458 *Geology* 26, 1139–1142. doi:10.1130/0091-7613(1998)026<1139:LTEOTO>2.3.CO;2.
- 459 Rijniens, L. A., Huinink, L. P., Kopinga, K., 2005. Experimental evidence of crystallization
460 pressure inside porous media. *Phys. Rev. Lett.* 94, 075503. doi:10.1103/PhysRevLett.
461 94.075503.
- 462 Robinson, P. T., Malpas, J., Zhou, M. F., Ash, C., Yang, J. S., Bai, W. J., 2005. Geochemistry
463 and origin of listwaenites in the Sartohay and Luobnsa ophiolites, China. *Int. Geol. Rev.*
464 47, 177–202.
- 465 Røyne, A., Jamtveit, B., Mathiesen, J., Malthe-Sørensen, A., 2008. Controls on rock weather-
466 ing rates by reaction-induced hierarchical fracturing. *Earth Planet. Sci. Lett.* 275, 364–369.
467 doi:10.1016/j.epsl.2008.08.035.
- 468 Santti, J., Kontinen, A., Sorjonen-Ward, P., Johanson, B., Pakkanen, L., 2006. Metamorphism
469 and chromite in serpentinitized and carbinite-silica-altered peridotites of the Paleoprotero-
470 zoic Outokumpu-Jormua Ophiolite Belt, Eastern Finland. *Int. Geol. Rev.* 48, 494–546.
- 471 Schandl, E. S., Naldrett, A. J., 1992. CO₂ metasomatism of serpentinites south of Timmins,
472 Ontario. *Can. Mineral.* 30, 93–108.
- 473 Schandl, E. S., Wicks, F. J., 1993. Carbonate and associated alteration of ultramafic and rhy-
474 olitic rocks at the Hemingway Property, Kidd Creek Volcanic Complex, Timmins, Ontario.
475 *Econ. Geol.* 88, 1615–1635. doi:10.2113/gsecongeo.88.6.1615.
- 476 Scherer, G. W., 1999. Crystallization in pores. *Cem. Conc. Res.* 29, 1347–1358. doi:10.1016/
477 S0008-8846(99)00002-2.
- 478 Scherer, G. W., 2004. Stress from crystallization of salt. *Cem. Conc. Res.* 34, 1613–1624.
479 doi:10.1016/j.cemconres.2003.12.034.
- 480 Schramm, B., Devey, C., Gillis, K. M., Lackschewitz, K., 2005. Quantitative assesment of
481 chemical and mineralogical changes due to progressive low-temperature alteration of East
482 Pacific Rise basalts from 0 to 9 Ma. *Chem. Geol.* 218, 281–313. doi:10.1016/j.chemgeo.
483 2005.01.011.
- 484 Sprunt, E. S., Brace, W. F., 1974. Direct observations of microcavities in crystalline rocks. *Int.*
485 *J. Rock Mech. Min. Sci. and Geomech. Abstr.* 11, 139–150. doi:10.1016/0148-9062(74)
486 92874-5.
- 487 Stanger, G., 1985. Silicified serpentinite in the Semail nappe of Oman. *Lithos* 18, 13–22.
488 doi:10.1016/0024-4937(85)90003-9.
- 489 Tenthorey, E., Scholz, C. H., Aharonov, E., Léger, A., 1998. Precipitation scaling and diagenesis
490 1. Experimental results. *J. Geophys. Res.* 103, 23951–23967. doi:10.1029/98JB02229.
- 491 Ucurum, A., 2000. Listwaenites in Turkey: Perspectives on formation and precious metal
492 concentration with reference to occurrences in East-Central Anatolia. *Ofioliti* 25, 15–29.

- 493 Ucurum, A., Larson, L. T., 1999. Geology, base-precious metal concentration and genesis of
494 the silica-carbonate alteration (listwaenties) from late Cretaceous ophiolitic melanges at
495 central east Turkey. *Chemie Der Erde* 59, 77–104.
- 496 Walder, J., Hallet, B., 1985. A theoretical model of the fracture of rock during freezing. *Geol.*
497 *Soc. Am. Bull.* 96, 336–346. doi:10.1130/0016-7606(1985)96<336:ATMOTF>2.0.CO;2.
- 498 Wilde, A., Simpson, L., Hanna, S., 2002. Preliminary study of Cenozoic alteration and plat-
499 inum deposition in the Oman ophiolite. *J. Virtual Explorer* 6, 7–13.
- 500 Wong, T.-F., Fredrich, J. T., Gwanmesia, G. D., 1989. Crack aperture statistics and pore
501 space fractal geometry of Westerley Granite and Rutland Quartzite: Implications for an
502 elastic model of rock compressibility. *J. Geophys. Res.* 94, 10267–10278.
- 503 Wu, Y.-S., Ye, M., Sudicky, E. A., 2009. Fracture-flow-enhanced matrix diffusion in solute.
504 *Transp. Porous Med.* in press. doi:10.1007/s11242-009-9383-4.
- 505 Wu, Y.-S., Zhang, K., Liu, H.-H., 2006. Estimating large-scale fracture permeability of
506 unsaturated rock using barometric pressure data. *Vadose Zone Journal* 5, 1129–1142.
507 doi:10.2136/vzj2006.0015.
- 508 Yakobson, B. I., 1991. Morphology and rate of fracture in chemical decomposition of solids.
509 *Phys. Rev. Lett.* 67, 1590 – 1593. doi:10.1103/PhysRevLett.67.1590.
- 510 Yund, R. A., 1997. Rates of grain boundary diffusion through enstatite and forsterite reaction
511 rims. *Contrib. Mineral. Petrol.* 126, 224–236. doi:10.1007/s004100050246.

512 **Appendices**

513 **A. Non-dimensionalisation**

The problem has just two non-dimensional parameters, Λ and Θ , defined by

$$\Lambda = \frac{\kappa}{D} \left(\frac{K_c}{\beta E} \right)^4, \quad \Theta = \frac{w_0}{rb_0}. \quad (26)$$

514 In presenting the final results, it is convenient to non-dimensionalise on the natural length
515 scale that arises in the fracture criterion (15), namely $(K_c/\beta E)^2$. Non-dimensional front
516 velocities and crack lengths can be defined using this length scale as

$$\eta = \frac{v}{D} \left(\frac{K_c}{\beta E} \right)^2, \quad \zeta = L \left(\frac{\beta E}{K_c} \right)^2. \quad (27)$$

517 Non-dimensionally, the aim of the analysis is to find $\eta(\Lambda, \Theta)$ and $\zeta(\Lambda, \Theta)$. The fracture
518 criterion (15) takes the simple form

$$1 = \zeta^{1/2} b'(0), \quad (28)$$

519 where $b' = b/b_0$ is a rescaled concentration.

520 While non-dimensionalising on $(K_c/\beta E)^2$ is convenient for the final results and the fracture
521 criterion, it is cumbersome for reaction-diffusion part of the problem, as that problem does
522 not directly contain the elastic parameters. A more convenient length scale for the reaction-
523 diffusion problem is D/v , and we introduce non-dimensional variables γ and λ as

$$\gamma = \frac{D\kappa}{v^2} = \frac{\Lambda}{\eta^2}, \quad \lambda = \frac{vL}{D} = \eta\zeta. \quad (29)$$

Introducing a rescaled concentration $w' = w/w_0$, a rescaled reaction rate $Q' = Q/\kappa b_0$, and a
non-dimensional co-ordinate $x' = xv/D$, the reaction-diffusion problem becomes

$$-\frac{dw'}{dx'} = \frac{d^2w'}{dx'^2} - \frac{\gamma}{\Theta} Q', \quad (30)$$

$$-\frac{db'}{dx'} = \gamma Q', \quad (31)$$

$$w'(0) = 1, \quad w'(\infty) = 0, \quad (32)$$

$$b'(\infty) = 0, \quad (33)$$

524

$$Q' = w'(1 - b'). \quad (34)$$

525 The strategy for solution of the above equations is as follows: The reaction-diffusion problem
526 (30-34) determines $\lambda(\gamma, \Theta)$ and $b'(0; \gamma, \Theta)$ where $\lambda(\gamma, \Theta)$ is the non-dimensional length scale
527 over which $b'(x'; \gamma, \Theta)$ decays, and $b'(0; \gamma, \Theta)$ is the value of $b'(x'; \gamma, \Theta)$ at the front. The
528 relationships between the different non-dimensional parameters (29) and the non-dimensional
529 fracture criterion (28) can then be used to find $\eta(\Lambda, \Theta)$ and $\zeta(\Lambda, \Theta)$.

530 **B. The reaction-diffusion problem**

From now on, we will drop primes and work solely with non-dimensional variables. The reaction-diffusion system (30-34) can be integrated once to give

$$\frac{dw}{dx} = -w - \frac{1}{\Theta}b, \quad (35)$$

$$\frac{db}{dx} = -\gamma Q = -\gamma w(1-b), \quad (36)$$

with boundary conditions

$$w(0) = 1, \quad w(\infty) = 0. \quad (37)$$

531 This is a second order non-linear two-point boundary value problem. For the connection with
 532 the fracture mechanics problem, we want to find $\lambda = \lambda(\gamma, \Theta)$ (the length scale over which b
 533 decays) and $b(0) = b(0; \gamma, \Theta)$ (the magnitude of b at the front). For moderate values of γ and
 534 Θ the above problem is easy to solve numerically. For very large or very small values of γ
 535 and Θ numerical solutions are more difficult. However, in these cases asymptotic solutions
 536 provide a very good approximation.

537 Numerical solutions showing typical concentration profiles are shown in Figure 5. From
 538 such profiles it is straightforward to calculate λ and $b(0)$. Shown in Figures 6 and 7 are
 539 contour plots showing the behaviour of λ and $b(0)$ as a function of γ and Θ .

540 *B.1. Asymptotic solutions*

541 There are a number of simple asymptotic approximations to the governing equations valid
 542 in certain parameter regimes. They provide simple analytic expressions for λ and $b(0)$ in the
 543 relevant regimes.

544 *B.1.1. Linearisation: Regimes 1 and 2*

The simplest asymptotic solution arises when we linearise the governing equations, namely

$$\frac{dw}{dx} = -w - \frac{1}{\Theta}b, \quad (38)$$

$$\frac{db}{dx} = -\gamma w. \quad (39)$$

545 Such an approximation will be justified provided $b \ll 1$. The above equations are easily
 546 integrated to give

$$w = e^{-mx}, \quad b = \frac{\gamma}{m}e^{-mx}, \quad (40)$$

where

$$m = \frac{-1 + \sqrt{1 + 4\gamma/\Theta}}{2}. \quad (41)$$

547 Hence

$$\lambda = \frac{1}{m}, \quad b(0) = \frac{\gamma}{m}. \quad (42)$$

These expressions can be further simplified if we assume either $\gamma \gg \Theta$ or $\gamma \ll \Theta$. Call $\gamma \gg \Theta$ regime 1, and $\gamma \ll \Theta$ regime 2. In regime 1 we have $m \sim (\gamma/\Theta)^{1/2}$ and

$$w = e^{-x(\gamma/\Theta)^{1/2}}, \quad b = (\gamma\Theta)^{1/2} e^{-x(\gamma/\Theta)^{1/2}}, \quad (43)$$

$$\lambda = \left(\frac{\Theta}{\gamma}\right)^{1/2}, \quad b(0) = (\gamma\Theta)^{1/2}. \quad (44)$$

548 Consistency of the approximation ($b \ll 1$) implies that regime 1 is the region where $\Theta \ll \gamma \ll$
549 Θ^{-1} .

In regime 2 we have $m \sim 1$ and

$$w = e^{-x}, \quad b = \gamma e^{-x}, \quad (45)$$

$$\lambda = 1, \quad b(0) = \gamma. \quad (46)$$

550 Consistency ($b \ll 1$) implies that regime 2 is the region where $\gamma \ll 1$ and $\gamma \gg \Theta$.

551 *B.1.2. Regime 3*

Another approximation to the governing equations that can be integrated analytically is

$$\frac{dw}{dx} = -w, \quad (47)$$

$$\frac{db}{dx} = -\gamma w (1 - b), \quad (48)$$

and will be valid provided $b \ll \Theta w$. The solution is

$$w = e^{-x}, \quad (49)$$

$$b = 1 - \exp(-\gamma e^{-x}). \quad (50)$$

If $\gamma \ll 1$ then this reduces to regime 2, where $b = \gamma e^{-x}$. Assume the opposite here, $\gamma \gg 1$. Then

$$\lambda = \log \gamma, \quad (51)$$

$$b(0) = 1. \quad (52)$$

552 With this approximation the concentration profile for b has a boundary layer structure, where
553 $b \sim 1$ until $x \sim \lambda$. The boundary layer thickness is order 1. Consistency ($b \ll \Theta w$) implies
554 that regime 3 is the region where $1 \ll \gamma \ll \Theta$.

555 *B.1.3. Regime 5*

Consider the approximate set of equations

$$\frac{dw}{dx} = -\frac{1}{\Theta} b, \quad (53)$$

$$\frac{db}{dx} = -\gamma w (1 - b), \quad (54)$$

556 which are valid if $\Theta w \ll b$. If $\gamma\Theta \ll 1$ this reduces to regime 1. Assume the opposite here,
 557 that $\gamma\Theta \gg 1$. The above can be combined to give

$$\frac{\Theta}{\gamma} \frac{d^2 w}{dx^2} - \Theta w \frac{dw}{dx} - w = 0. \quad (55)$$

558 It is helpful to introduce a rescaled co-ordinate $y = x/\Theta$,

$$\frac{1}{\gamma\Theta} \frac{d^2 w}{dy^2} - w \frac{dw}{dy} - w = 0. \quad (56)$$

559 $\gamma\Theta \gg 1$ is a singular perturbation of the above equation. In this case, the solution has the
 560 approximate form

$$w = \begin{cases} 1 - x/\Theta, & x < \Theta, \\ 0, & x > \Theta. \end{cases} \quad (57)$$

561

$$b = \begin{cases} 1, & x < \Theta, \\ 0, & x > \Theta. \end{cases} \quad (58)$$

562 Thus

$$\lambda = \Theta, \quad b(0) = 1. \quad (59)$$

563 In detail, there is a boundary layer in the solution at $x = \lambda$, with a thickness of order $(\Theta/\gamma)^{1/2}$.
 564 Consistency ($\Theta w \ll b$) implies that regime 5 is the region where $\gamma^{-1} \ll \Theta \ll 1$.

565 *B.1.4. Regime 4*

566 The remaining unexplored parameter regime has $1 \ll \Theta \ll \gamma$. We again expect a boundary
 567 layer behaviour. However, in this regime both terms in (35) are important. Consider (35)
 568 with $b = 1$,

$$\frac{dw}{dx} = -w - \frac{1}{\Theta}, \quad (60)$$

569 which has solution

$$w = \left(1 + \frac{1}{\Theta}\right) e^{-x} - \frac{1}{\Theta}. \quad (61)$$

570 This is zero when $x = \log(1 + \Theta)$, and this is where the boundary layer for b is expected. If
 571 $\Theta \ll 1$ this returns to regime 5, whereas if $\Theta \gg 1$ we have

$$\lambda = \log \Theta, \quad b(0) = 1. \quad (62)$$

572 The initial balance of terms has $\Theta w \gg b$ as in regime 3, but for $x \gg 1$ we have $\Theta w \ll b$ as
 573 in regime 5. The boundary layer structure at $x = \lambda$ should be similar to regime 4, with an
 574 order $(\Theta/\gamma)^{1/2}$ thickness.

575 [Table 2](#) summarises the different asymptotic regimes for the reaction-diffusion problem,
 576 and a regime diagram is shown in [Figure 8](#).

577 **C. The fracture criterion**

578 Once $\lambda(\gamma, \Theta)$ and $b(0; \gamma, \Theta)$ are known, all that remains is the fracture criterion (28),

$$1 = \zeta^{1/2} b(0), \quad (63)$$

579 and the additional relationships (29)

$$\gamma = \Lambda/\eta^2, \quad \zeta = \lambda/\eta. \quad (64)$$

580 These can be combined to give

$$1 = \left(\frac{\lambda(\Lambda/\eta^2, \Theta)}{\eta} \right)^{1/2} b(0; \Lambda/\eta^2, \Theta), \quad (65)$$

581 which is an expression that can be inverted to find $\eta(\Lambda, \Theta)$. Moreover, the fracture criterion
582 (63) can be rewritten as

$$\zeta = (b(0, \Lambda/\eta^2, \Theta))^{-2}, \quad (66)$$

583 and thus we can find $\zeta(\Lambda, \Theta)$ given $\eta(\Lambda, \Theta)$. This completes the problem; Numerical solutions
584 are shown in Figures 2 and 3. Asymptotic solutions are given in Table 3, with a regime
585 diagram in Figure 4. The final dimensional results are given in Table 1.

586 **D. Related problems**

587 *D.1. Decomposition of solids: Jakobson 1991*

588 In this work we have used a very simple fracture criterion, given in dimensional form by

$$K_c = \sigma(0)L^{1/2}, \quad (67)$$

589 where the crack length L was chosen to be length scale δ over which $\sigma(x)$ decays.

590 Similar results can be obtained from other fracture criterion. For example, in the model
591 of decomposition of solids by Jakobson (1991), the following fracture criterion was used

$$K_c = 2 \left(\frac{L}{\pi} \right)^{1/2} \int_0^L \frac{\sigma(x)}{(L^2 - x^2)^{1/2}} dx. \quad (68)$$

592 As it stands, the above equation produces a family of solutions relating v to L . In Jakobson
593 (1991)'s model, the final choice of L is made by a dynamical hypothesis that assumes v takes
594 its maximum value. In fact, Jakobson (1991)'s criterion can be related to the simple one used
595 here. Let us suppose that $\sigma(x)$ can be written as

$$\sigma(x) = \sigma(0)g(x/\delta), \quad (69)$$

where δ is the characteristic length scale over which $\sigma(x)$ decays, and $g(y)$ is some decaying
function of y that is independent of any parameters. Then

$$\begin{aligned} K_c &= 2 \left(\frac{L}{\pi} \right)^{1/2} \int_0^L \frac{\sigma(0)g(x/\delta)}{(L^2 - x^2)^{1/2}} dx \\ &= \sigma(0)\delta^{1/2} \cdot 2 \left(\frac{\rho}{\pi} \right)^{1/2} \int_0^\rho \frac{g(y)}{(\rho^2 - y^2)^{1/2}} dy \\ &= \sigma(0)\delta^{1/2} f(\rho) \end{aligned} \quad (70)$$

where $\rho = L/\delta$. The dynamical hypothesis that v is maximal implies that ρ must be an extremum for $f(\rho)$. Let $\rho = \rho_c$ be this extremum, with $f(\rho_c) = f_c$ its extreme value. Since $f(\rho)$ is assumed not to depend on any of the parameters in the problem, ρ_c and f_c will simply be some order 1 numbers. Thus Yakobson's approach leads to

$$L = \rho_c \delta, \quad (71)$$

$$K_c = f_c \sigma(0) \delta^{1/2}, \quad (72)$$

which is exactly the same as the simplified criterion used here up to order 1 constants. In detail, Yakobson's particular problem has

$$g(y) = e^{-y}, \quad (73)$$

$$f(y) = \sqrt{\pi y} (I_0(y) - L_0(y)), \quad (74)$$

$$\rho_c = 0.917291, \quad (75)$$

$$f_c = 0.986713, \quad (76)$$

596 where I_0 is the zeroth order modified Bessel function of the first kind, and L_0 is the zeroth
597 order modified Struve function.

598 [Yakobson \(1991\)](#)'s concentration problem is the following

$$-v \frac{dc}{dx} = D \frac{d^2c}{dx^2}. \quad (77)$$

599 with boundary conditions

$$D \frac{dc}{dx}(0) = k_e c(0), \quad c(\infty) = c_\infty, \quad (78)$$

600 where k_e is an evaporation constant. The stress is related through

$$\sigma(x) = \beta E (1 - c(x)/c_\infty). \quad (79)$$

601 There is just one non-dimensional parameter in this problem, namely

$$\Delta = \frac{k_e}{D} \left(\frac{K_c}{\beta E} \right)^2. \quad (80)$$

As before, non-dimensional variables can be introduced as

$$\eta = \frac{v}{D} \left(\frac{K_c}{\beta E} \right)^2, \quad \zeta = L \left(\frac{\beta E}{K_c} \right)^2, \quad (81)$$

$$\mu = \frac{k_e}{v} = \frac{\Delta}{\eta}, \quad \lambda = \frac{Lv}{D} = \eta \zeta, \quad (82)$$

602 Non-dimensionally ($x' = xv/D$), the concentration field is

$$1 - c'(x') = \frac{e^{-x'}}{1 + \mu^{-1}}. \quad (83)$$

603 Thus

$$\lambda = 1, \quad 1 - c'(0) = \frac{1}{1 + \mu^{-1}}. \quad (84)$$

604 The non-dimensional fracture criterion is

$$1 = \zeta^{1/2} (1 - c'(0)), \quad (85)$$

and the relationships in (82) imply

$$\eta \left(1 + \frac{\eta}{\Delta}\right)^2 = 1, \quad (86)$$

$$\zeta = \eta^{-1}. \quad (87)$$

There are two asymptotic regimes. If $\Delta \gg 1$ (“brittle fracturing”) then

$$\eta = 1, \quad v = D \left(\frac{\beta E}{K_c}\right)^2, \quad (88)$$

$$\zeta = 1, \quad L = \left(\frac{K_c}{\beta E}\right)^2, \quad (89)$$

which is similar to regimes 4 and 5 in the reaction-diffusion model. If $\Delta \ll 1$ (“evaporation controlled”)

$$\eta = \Delta^{2/3}, \quad v = D^{1/3} \left(\frac{\beta E k_e}{K_c}\right)^{2/3} \quad (90)$$

$$\zeta = \Delta^{-2/3}, \quad L = \left(\frac{DK_c}{\beta E k_e}\right)^{2/3}, \quad (91)$$

605 which is similar in form to regime 2 in the reaction-diffusion model. The scalings above are also
 606 seen in more sophisticated models, such as those by [Boeck et al. \(1999\)](#) and [Malthe-Sørensen
 607 et al. \(2006\)](#)).

608 *D.2. Spheroidal weathering: Fletcher et al. 2006*

609 [Fletcher et al. \(2006\)](#) have also developed a model that couples a reaction-diffusion equa-
 610 tion to a fracture mechanics problem to study chemical weathering. In fact, their model is
 611 very closely related to that considered here. [Table 4](#) provides a mapping between the notation
 612 used by [Fletcher et al. \(2006\)](#) and that used here. Their reaction-diffusion problem has the
 613 slight difference that their reaction rate $\propto w^{1/4}a$ with a cut-off for low concentrations, rather
 614 than reaction rate $\propto wa$ used here. The fracture mechanics is also treated a little differently:
 615 Fracturing is considered as an episodic process that occurs when the integrated elastic strain
 616 energy reaches a threshold value given by the surface energy of fracture. After each fracturing
 617 event the front moves forward to the cut-off point for the reaction. Thus the length scale for
 618 fracturing (crack spacing) in the [Fletcher et al. \(2006\)](#) model is also set by the length scale
 619 over which a concentration profile decays, but it is the concentration profile of the water w
 620 rather than that of the product b which is used. In regimes 1, 2, and 5 the length scales for
 621 decay of product b and water w are the same, but in regimes 3 and 4 they are different, and in
 622 those regimes differences between our model and that of [Fletcher et al. \(2006\)](#) are expected.

623 A connection can be made with the simplified fracture criterion used here. The energy
 624 fracture criterion used by [Fletcher et al. \(2006\)](#) is

$$\int_0^L U(x) dx = 2\Gamma, \quad (92)$$

625 where Γ is the surface energy of fracture, and $U(x)$ is the elastic energy density. $U(x)$ is given
 626 by

$$U(x) = \frac{\sigma^2(x)}{E}. \quad (93)$$

627 There will also be a dependence on Poisson's ratio ν , but this depends on the specific details
 628 of the elastic problem, and has been neglected here. The surface energy of fracture can be
 629 related to the fracture toughness by

$$2\Gamma = \frac{K_c^2}{E}, \quad (94)$$

630 Again the ν dependence has been neglected. Thus the fracture criterion is

$$\int_0^L \sigma^2(x) dx = K_c^2. \quad (95)$$

631 Writing $\sigma(x) = \sigma(0)g(x/\delta)$ as in [\(69\)](#) yields

$$K_c = \mu_c \sigma(0) \delta^{1/2}, \quad (96)$$

632 where μ_c is

$$\mu_c = \left(\int_0^{L/\delta} g^2(y) dy \right)^{1/2}, \quad (97)$$

633 If the length scales for decay of the product b and water w are the same, then $L = \delta$, and μ_c
 634 is simply some order 1 constant. Thus the two fracturing criteria are equivalent in this case.

635 The two non-dimensional groups considered by [Fletcher et al. \(2006\)](#) can be related to
 636 those used here by

$$\Lambda_F = \frac{\Lambda}{\Theta}, \quad \alpha_F = \Lambda, \quad (98)$$

637 where subscript F refers to [Fletcher et al. \(2006\)](#)'s notation. Their numerics used $\Lambda_F = 0.0572$
 638 and $\alpha_F = 1.26 \times 10^{-7}$ ($\Lambda = 1.26 \times 10^{-7}$ and $\Theta = 2.20 \times 10^{-6}$), which suggests they should
 639 be in regime 1. By conducting numerical simulations of their time-dependent problem they
 640 found that a steady state is reached, with the front propagating at a constant velocity. Their
 641 distance between fractures is given by [\(\(18\) of Fletcher et al. \(2006\)\)](#)

$$W_F \approx 1.44 x_F^* \Lambda_F^{-1/2} = 1.44 \left(\frac{K_c}{\beta E} \right)^2 \Lambda^{-1/2} \Theta^{1/2}, \quad (99)$$

642 which is the same scaling as regime 1,

$$L = \left(\frac{K_c}{\beta E} \right)^2 \Lambda^{-1/2} \Theta^{1/2}. \quad (100)$$

643 Their weathering advance rate $\omega_F = W_F/t_{F\text{crack}}$ ((22) of Fletcher et al. (2006)) is

$$\omega_F = 0.660 \frac{x_F^*}{t_F^*} \Lambda_F^{-4/5} \alpha_F = 0.660 D \left(\frac{\beta E}{K_c} \right)^2 \Lambda^{1/5} \Theta^{4/5} \quad (101)$$

644 which is almost, but not quite, the same scaling as regime 1,

$$v = D \left(\frac{\beta E}{K_c} \right)^2 \Lambda^{1/4} \Theta^{3/4}. \quad (102)$$

645 The difference in the scalings is in the powers of Λ and Θ , which are 0.25 and 0.75 in the
 646 analysis here, but 0.2 and 0.8 for Fletcher et al. (2006). However, this difference might be
 647 explained by the fact that Fletcher et al. (2006)'s scalings are based on best fits to their
 648 numerical simulations rather than rigorous asymptotic analysis. If the same scalings were to
 649 hold, the corrected version of (22) of Fletcher et al. (2006) would be

$$\omega_F = 0.764 \frac{x_F^*}{t_F^*} \Lambda_F^{-3/4} \alpha_F, \quad (103)$$

i.e. a coefficient of -0.75 rather than -0.8 for Λ_F . Written out in full, Fletcher et al. (2006)'s expressions relating crack length and weathering advance rate would become (in their notation)

$$W = 1.44 \left(\frac{D\phi^m c_R}{r\tau\rho MSk f_0} \right)^{1/2}, \quad (104)$$

$$\omega = 0.764 (\rho MSk)^{1/4} \left(\frac{D\phi^m c_R}{r\tau f_0} \right)^{3/4} \left[\frac{E \left(\frac{f_0}{3} \frac{\Delta V}{V} \right)^2}{2\Gamma(1-\nu)} \right]^{1/2} V_{\text{FeO}}. \quad (105)$$

Regime	Range of validity	v	L
1	$\Theta^5 \ll \Lambda \ll \Theta$	$\frac{\beta E}{K_c} \kappa^{1/4} (D\Theta)^{3/4}$	$\left(\frac{D\Theta}{\kappa}\right)^{1/2}$
2	$\Lambda \ll 1, \Lambda \ll \Theta^5$	$D^{3/5} \left(\frac{\beta E \kappa}{K_c}\right)^{2/5}$	$\left(\frac{K_c D}{\beta E \kappa}\right)^{2/5}$
3	$1 \ll \Lambda \ll \Theta(\log \Theta)^2$	$2D \left(\frac{\beta E}{K_c}\right)^2 W\left(\frac{1}{2} \left(\frac{K_c}{\beta E}\right)^2 \left(\frac{\kappa}{D}\right)^{1/2}\right)$	$\left(\frac{K_c}{\beta E}\right)^2$
4	$1 \ll \Theta, \Theta(\log \Theta)^2 \ll \Lambda$	$D \left(\frac{\beta E}{K_c}\right)^2 \log \Theta$	$\left(\frac{K_c}{\beta E}\right)^2$
5	$\Theta \ll 1, \Theta \ll \Lambda$	$D \left(\frac{\beta E}{K_c}\right)^2 \Theta$	$\left(\frac{K_c}{\beta E}\right)^2$

Table 1: A summary of the asymptotic regimes for the model in dimensional units. Here $W(z)$ is the Lambert function (the solution of $z = W(z) \exp(W(z))$).

Regime	Range of validity	λ	$b(0)$
1	$\Theta \ll \gamma \ll \Theta^{-1}$	$\Theta^{1/2}\gamma^{-1/2}$	$\Theta^{1/2}\gamma^{1/2}$
2	$\gamma \ll 1, \gamma \ll \Theta$	1	γ
3	$1 \ll \gamma \ll \Theta$	$\log \gamma$	1
4	$1 \ll \Theta \ll \gamma$	$\log \Theta$	1
5	$\gamma^{-1} \ll \Theta \ll 1$	Θ	1

Table 2: A summary of the asymptotic regimes for the reaction-diffusion problem.

Regime	Range of validity	η	ζ	$b(0)$
1	$\Theta^5 \ll \Lambda \ll \Theta$	$\Lambda^{1/4} \Theta^{3/4}$	$\Lambda^{-1/2} \Theta^{1/2}$	$\Lambda^{1/4} \Theta^{-1/4}$
2	$\Lambda \ll 1, \Lambda \ll \Theta^5$	$\Lambda^{2/5}$	$\Lambda^{-2/5}$	$\Lambda^{1/5}$
3	$1 \ll \Lambda \ll \Theta(\log \Theta)^2$	$2W(\Lambda^{1/2}/2)$	1	1
4	$1 \ll \Theta, \Theta(\log \Theta)^2 \ll \Lambda$	$\log \Theta$	1	1
5	$\Theta \ll 1, \Theta \ll \Lambda$	Θ	1	1

Table 3: A summary of the asymptotic regimes for the full problem. Here $W(z)$ is the Lambert function (the solution of $z = W(z) \exp(W(z))$).

Our model	Fletcher et al. notation	Fletcher et al. value
E	E	10^{11} Pa
K_c	$\sqrt{\frac{2\Gamma E}{1-\nu}}$	7.30×10^6 Pa m ^{1/2}
β	$\frac{f_0 \Delta V}{3(1-\nu) V}$	1.11×10^{-3}
b_0	$\frac{f_0}{V_{\text{FeO}}}$	4170 mol m ⁻³
w_0	$\frac{\phi c_R}{V_{\text{FeO}}}$	2.3×10^{-3} mol m ⁻³
κ	$\rho M S k V_{\text{FeO}}$	1.12×10^{-10} s ⁻¹
r	r	0.25
s	1	1
D	$\frac{D\phi^{m-1}}{\tau}$	1.67×10^{-8} m ² s ⁻¹
v	ω	3.18×10^{-12} m s ⁻¹
L	W	0.026 m
Λ	α	1.26×10^{-7}
Θ	$\frac{\alpha}{\Lambda}$	2.20×10^{-6}

Table 4: A mapping between the notation used here and that of [Fletcher et al. \(2006\)](#). The value of α quoted above ($\alpha = 1.26 \times 10^{-7}$) differs from that directly quoted by [Fletcher et al. \(2006\)](#) ($\alpha = 6.32 \times 10^{-9}$) due to typographical errors.

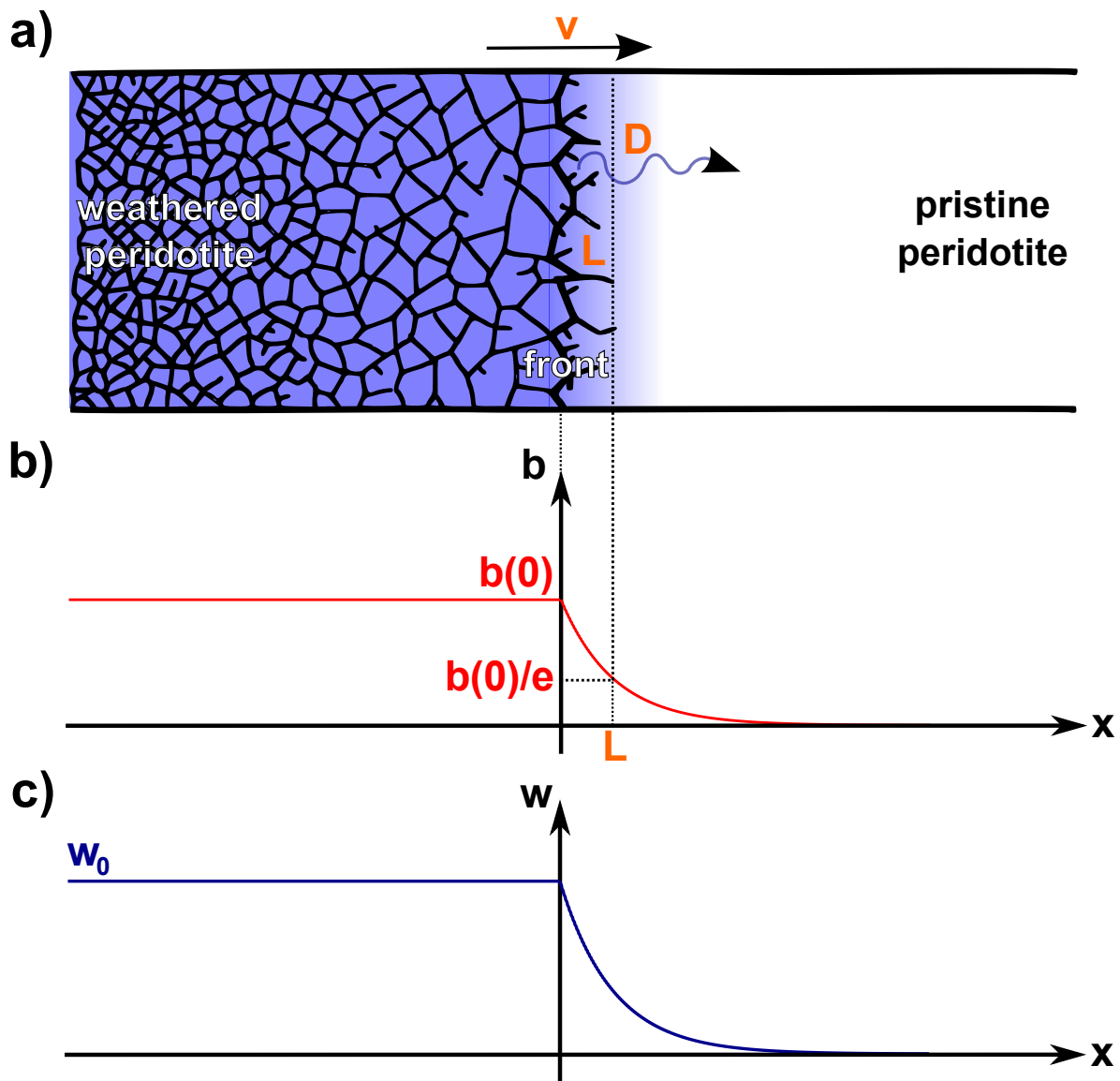


Figure 1: Schematic diagram of the model. a) depicts the model geometry, with blue shading reflecting water concentration. b) and c) depict the concentration profiles of product b and mobile phase w respectively. The exact profiles depend on the choice of parameters; shown here are typical exponential profiles for Regime 1.

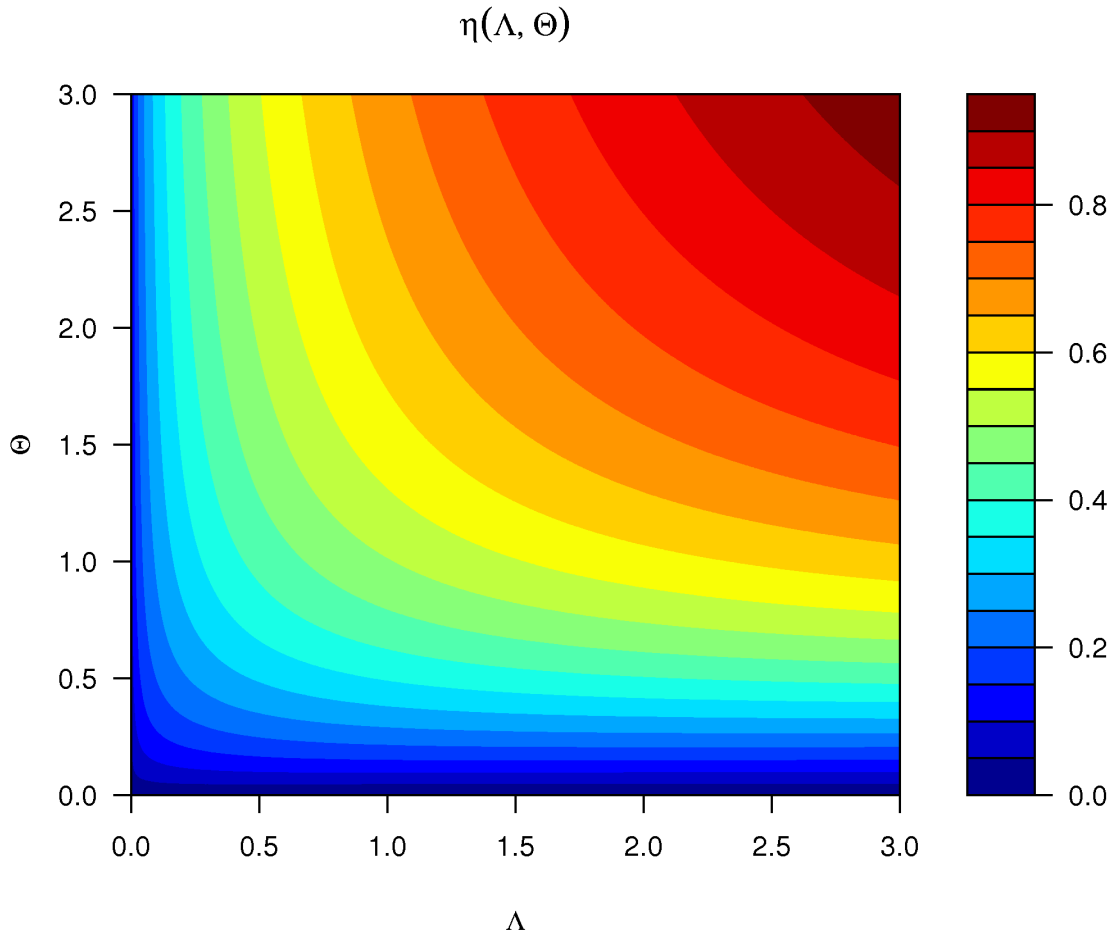


Figure 2: Results of numerical solutions showing $\eta = (v/D)(K_c/\beta E)^2$ (a non-dimensional front velocity) as a function of Λ and Θ .

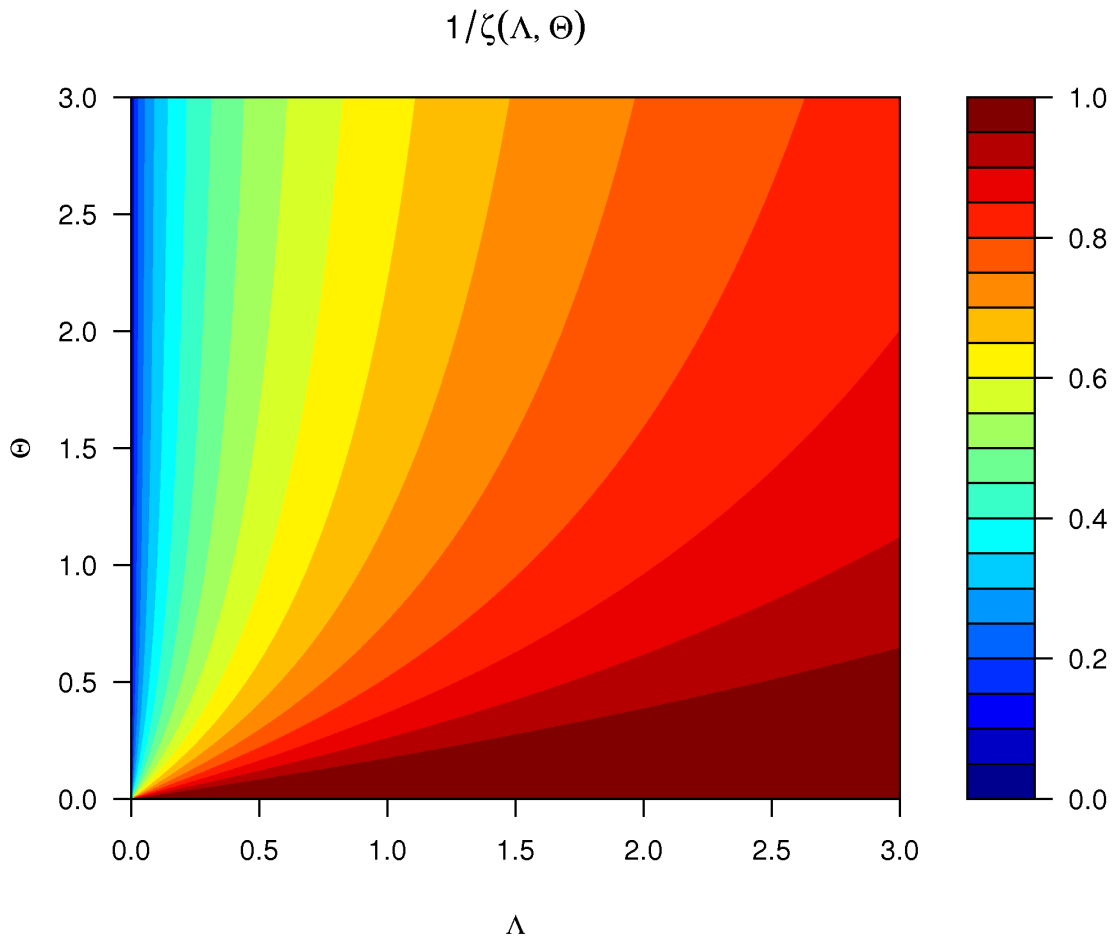


Figure 3: Results of numerical solutions showing $1/\zeta$ as a function of Λ and Θ . $\zeta = L(\beta E/K_c)^2$ is a non-dimensional crack length. It is more convenient to plot $1/\zeta$ rather than ζ due to the singular behaviour of ζ near $\Lambda = 0$.

Asymptotic regimes

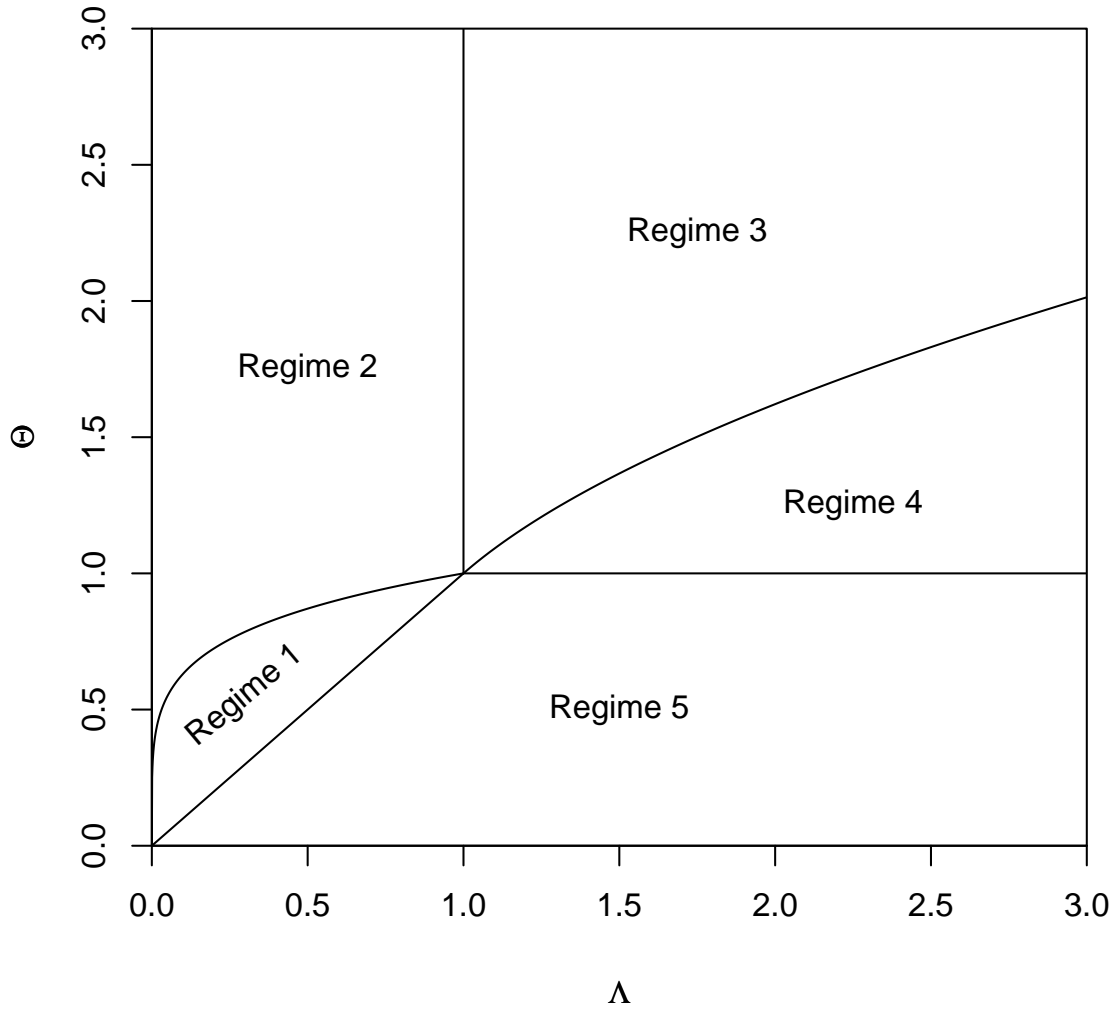


Figure 4: A map of the asymptotic regimes in terms of Λ and Θ .

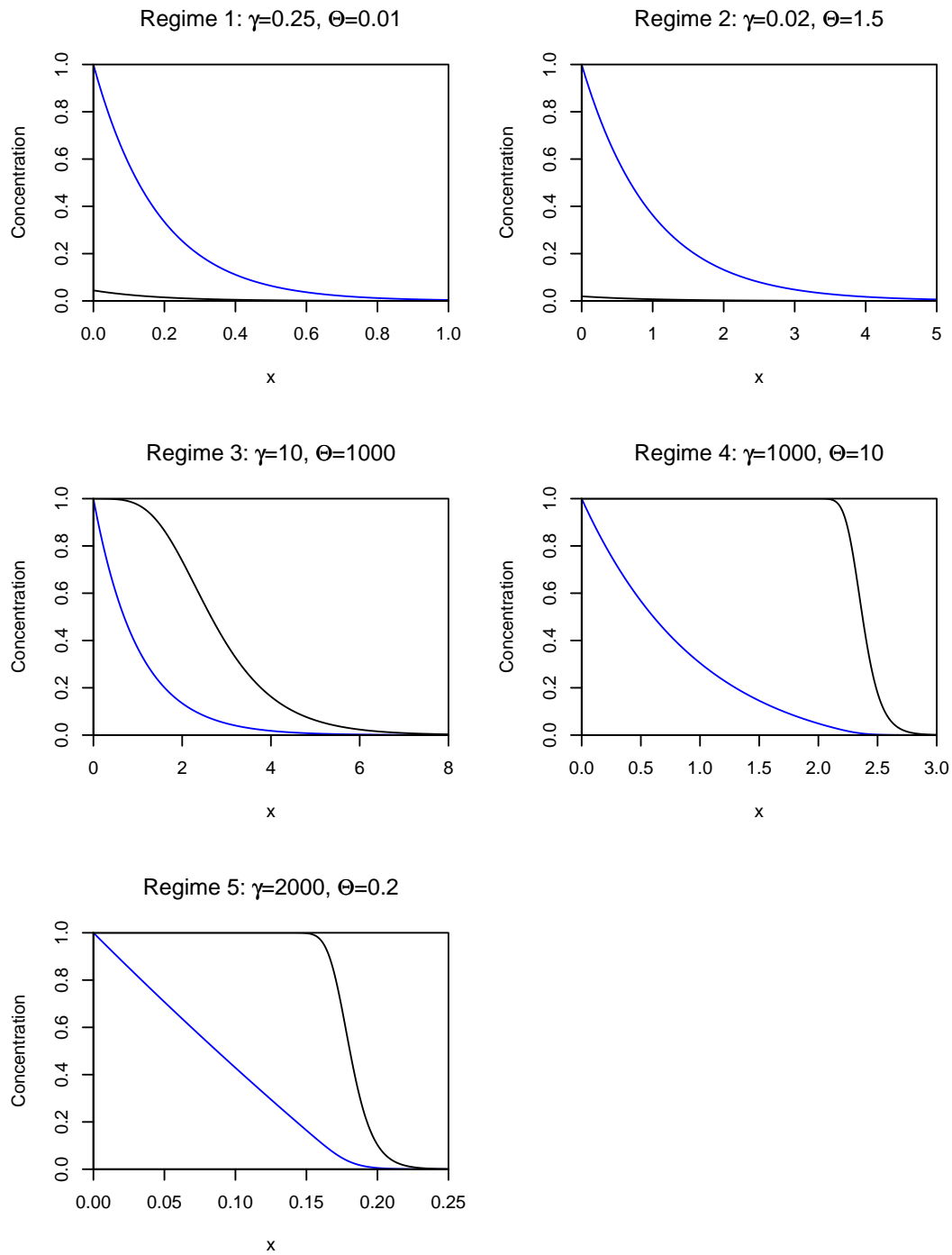


Figure 5: Numerical solutions of the non-dimensional reaction-diffusion equation. Parameters have been chosen to give examples of the different asymptotic regimes. Blue curves are the mobile phase w , black curves are the immobile product b .

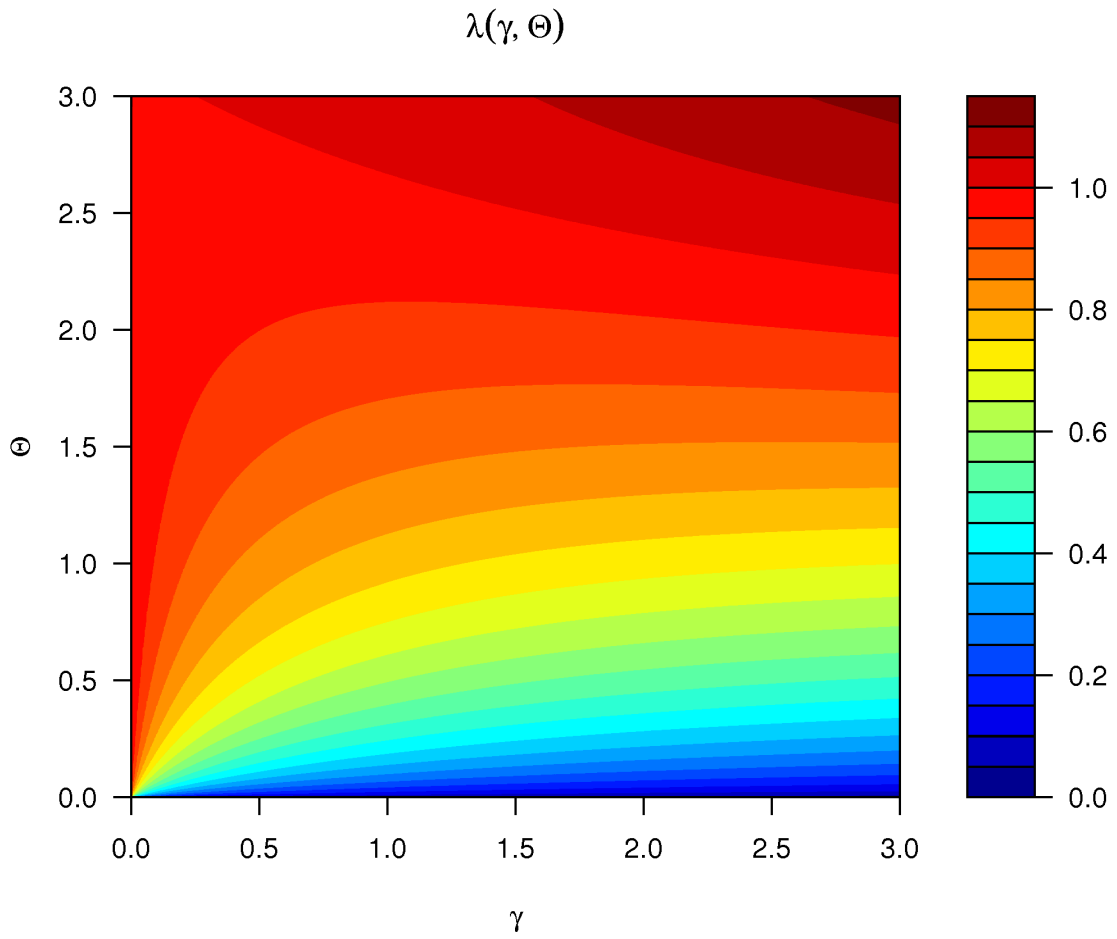


Figure 6: Results of numerical solutions showing $\lambda = Lv/D$ as a function of γ and Θ .

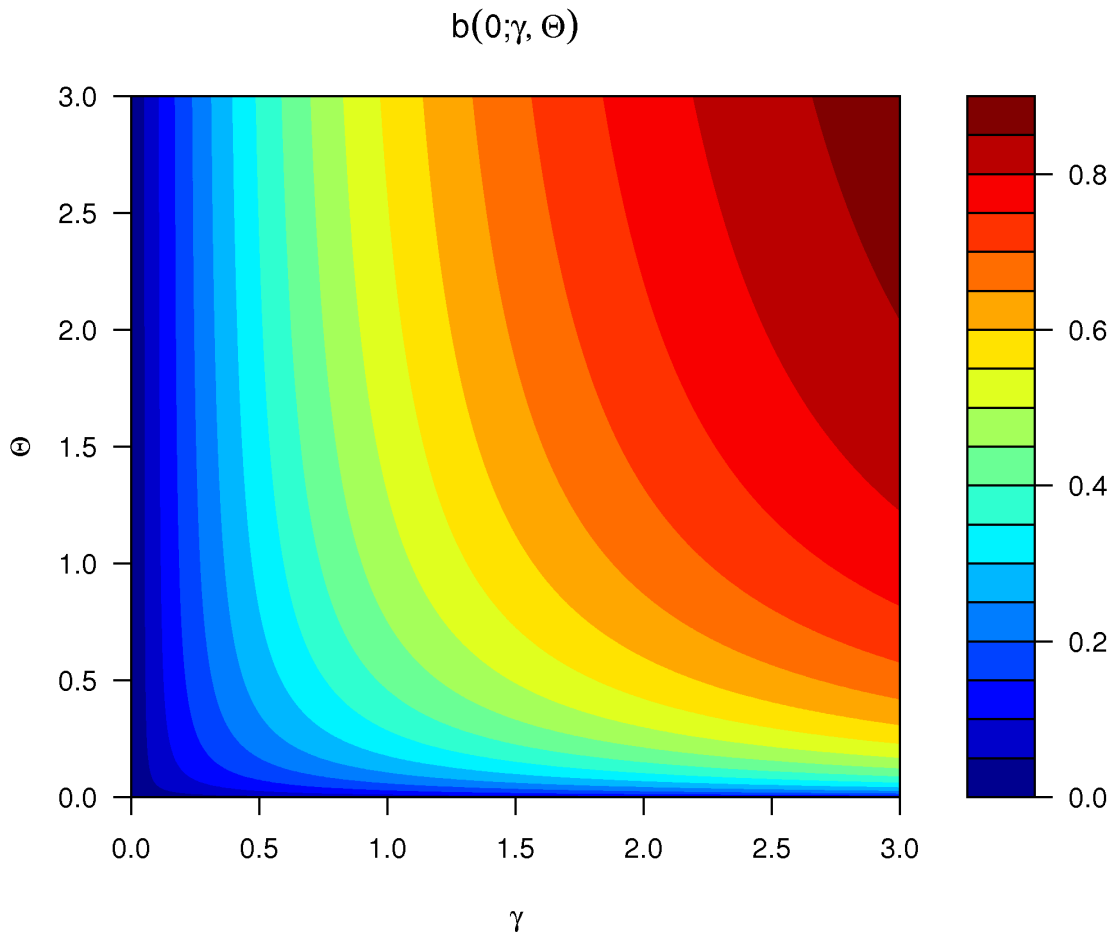


Figure 7: Results of numerical solutions showing $b(0)$ as a function of γ and Θ .

Asymptotic regimes

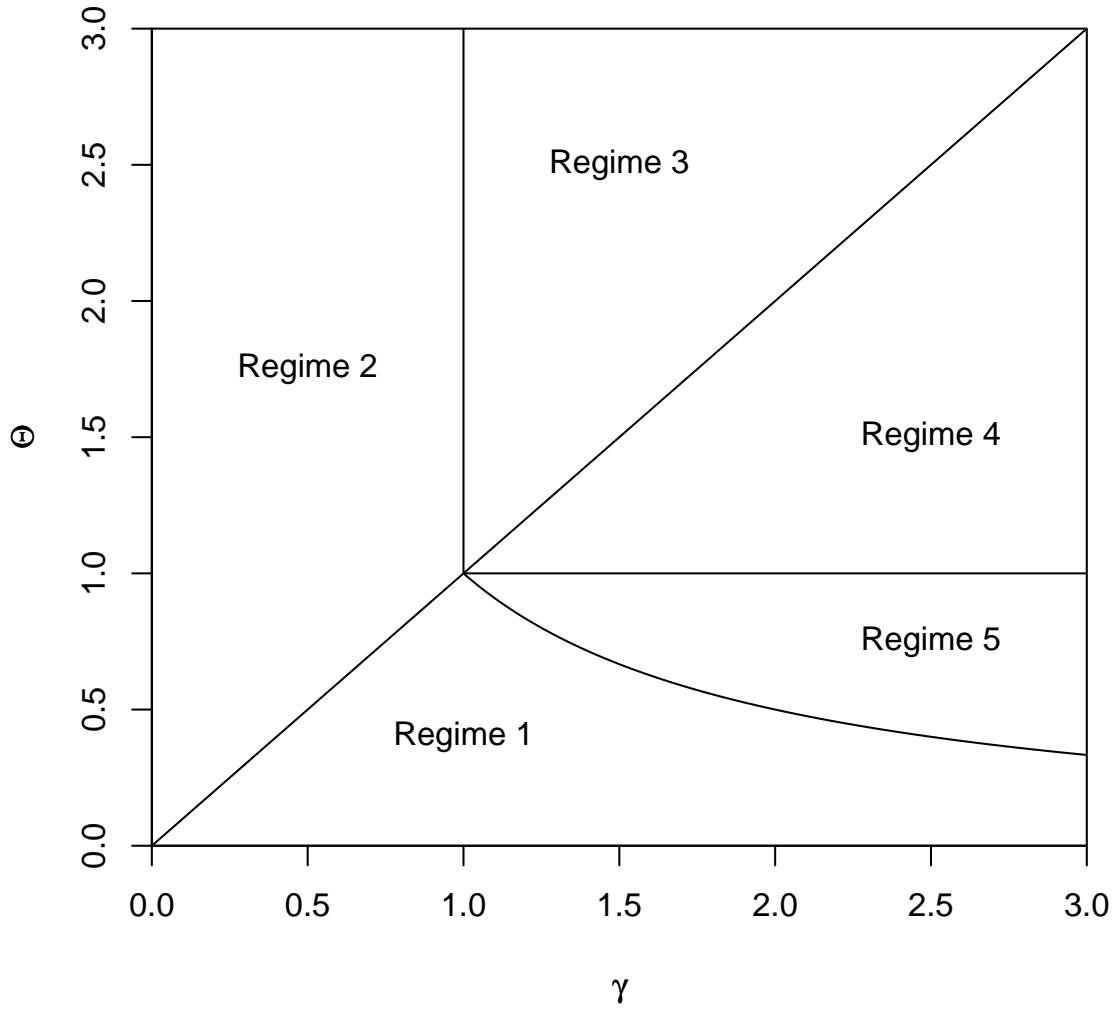


Figure 8: A map of the asymptotic regimes for the reaction-diffusion problem in terms of γ and Θ .